DeepWind Deliverable

Grant Agreement number: 256769

Project title: **Future Deep Sea Wind Turbine Technologies**

Deliverable No.: **D6.2**

Deliverable title: **Technical Report on Refined Numerical Modelling**

Deliverable status: **Report**

Name of lead beneficiary: **DHI**

Nature of deliverable: **R**

Dissemination level: **PU**

Due date from Annex 1: **M12**

Actual submission date: **31 October 2012**

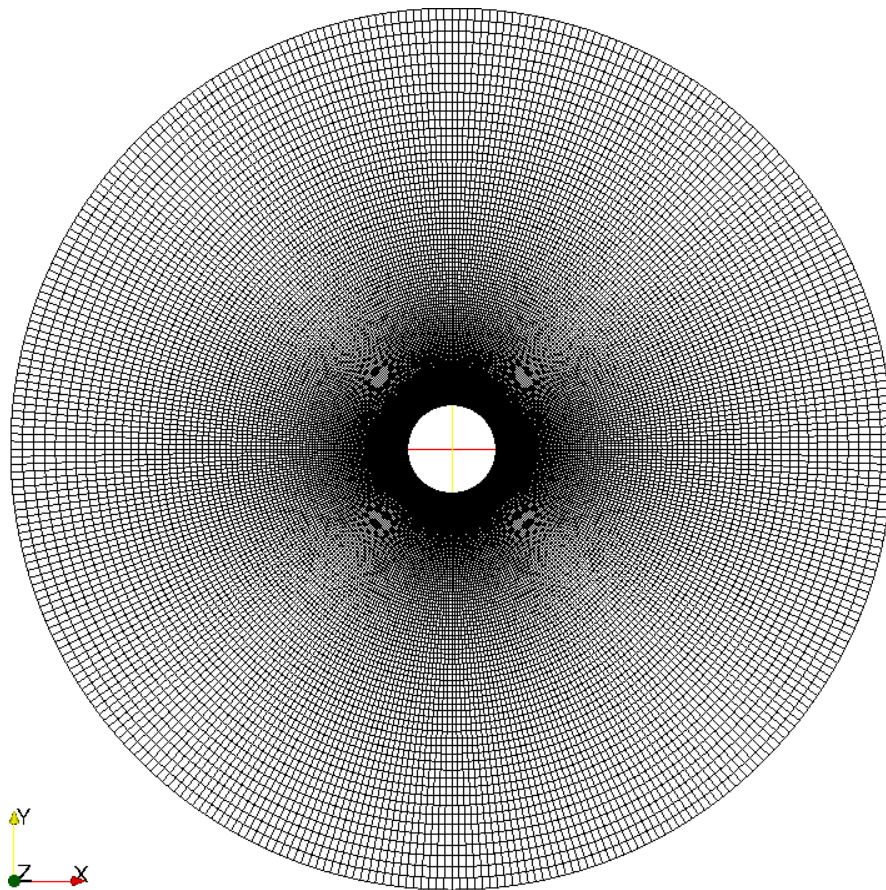**Quality check approval by:** *(signature)* **date:** 28/10 - 2012

256769 - DEEPWIND

Technical Report on Refined Numerical Modelling

Deliverable 6.2

256769 - DEEPWIND

Technical Report on Refined Numerical Modelling

Deliverable 6.2

This project was delivered under the DHI
Business Management System certified by
DNV to be in compliance with ISO 9001:
Quality Management System

256769 - DEEPWIND

Technical Report on Refined Numerical Modelling

Deliverable 6.2

October 2012

Client	Client's representative
EC-FP7-FET [ENERGY.2010.10.2-1]	Mr Thierry D'Estangtoi

Project				Project No			
DEEPWIND				11807547			
Authors				**Date**			
Stefan Carstensen				31 October 2012			
				Approved by			
				Jesper Fuchs Head of Projects, POT			
C	Report			SCA	JUF	JUF	31.10.12
B	Draft Report			SCA	EDC	JUF	30.03.12
A	Working Draft Report			SCA			
Revision	Description			By	Checked	Approved	Date

Key words	Classification
Cylinder Forces VAWT CFD Current, Waves, Rotation	☐ Open ☐ Internal ☒ Proprietary

Distribution		No of copies
EU:	Mr Thierry D'Estangtoi	PDF
	Partners	PDF
DHI:	SCA – XEM – JTS	PDF

CONTENTS

APPENDIX

A   Test Conditions and Force Coefficients

1   INTRODUCTION

This report is Deliverable 6.2 "Technical report on the numerical modelling" under Work Package 6 of the DEEPWIND project.

The DEEPWIND project is a collaborative research project on future deep sea wind turbine technologies which is partially funded by the European Commission (EC) through the 7th Framework Programme (FP7), EC-FP7-FET [ENERGY.2010.10.2-1]. Project work was started on 1 October 2010 after accession by DHI of Grant Agreement no: 256769 between the EC and the DEEPWIND consortium, which is coordinated by DTU Wind Energy (formerly RISØ DTU) and consists of DHI and 10 additional partners.

Work Package 6 of the DEEPWIND project addresses forces on a rotating circular cylinder in water. The circular cylinder represents the submerged part of the novel floating wind turbine concept described in /1/ and studied in the DEEPWIND project. The floating wind turbine concept, in the following denoted the DEEPWIND concept, is shown in Figure 1.1.
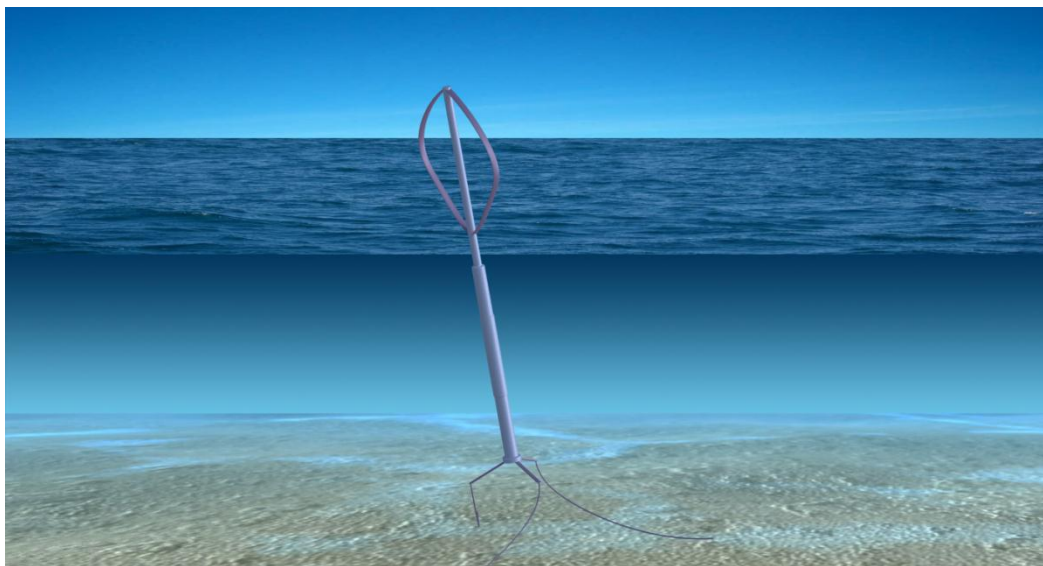
Figure 1.1   Artist's illustration of the DEEPWIND concept.

Work Package 6 utilises physical laboratory tests (Deliverable 6.1, see /7/) to establish the physics and address possible scaling effects with refined numerical modelling (Deliverable 6.2). The results are then analysed and parameterised as a basis for the engineering model (Deliverable 6.3). The present report describes the refined numerical modelling and results. The conclusion (Section 2) is kept short and expanded upon in Deliverable 6.3 ("Description of Engineering Model").

2   EXECUTIVE SUMMARY

Forces on a rotating circular cylinder in unsteady flow have been studied numerically with a computational fluid dynamics (CFD) code.

The results are consistent with the results from the physical model experiments reported in /7/ and show that the cross-flow (lift) force to a first approximation may be represented by a formulation similar to the well-known Morison formulation. The lift force is found to be almost in phase with the free-stream velocity and depends on the speed ratio between the surface speed of the cylinder and the surrounding flow velocity. The variation of the lift force with the phase of the wave motion was shown in /7/ to be predicted by potential flow theory for KC < 8. However, the magnitude of the lift force was substantially smaller than that predicted by potential flow theory. The magnitude of the lift force was found to be in the order of (0.5 to 2 times) the in-line hydrodynamic mass force. The hydrodynamic mass force is proportional to the acceleration which means that there is a phase difference of almost 90 degrees between the in-line force and the cross-flow force for KC < 8.

The in-line force was also investigated. The cylinder rotation was found to have a limited effect on the in-line force for small KC numbers and wave-dominated combined wave and current

The friction torque opposing the cylinder rotation was measured in stagnant water and for various combined wave and current conditions. The friction torque in stagnant water was shown to compare with previous studies; and the friction torque opposing the cylinder rotation, under wave action, was found to be of the same order of magnitude as that for rotation alone.

3 NUMERICAL MODEL

This section gives a brief description of the computational model used throughout the present work. For brevity only equations and boundary conditions are discussed, and for details of the (finite volume) numerical schemes employed the reader is referred to standard textbooks on the subject.

3.1 Model Description

The numerical model is an in-house extension of a standard solver in the OpenFOAM CFD toolbox. The extension allows the flow to be driven by an unsteady and non-zero mean body force, as described below, and thereby simulating combined wave and current action.

The numerical model solves the incompressible Reynolds-averaged Navier-Stokes equations:

$$\frac{\partial u_i}{\partial t} + u_j \frac{\partial u_i}{\partial x_j} = -\frac{1}{\rho}\frac{\partial p}{\partial x_i} + \frac{\partial}{\partial x_j}\left[\nu\left(\frac{\partial u_i}{\partial x_j} + \frac{\partial u_j}{\partial x_i}\right) + \frac{\tau_{ij}}{\rho}\right] + F_{Bi}$$

Combined with the local continuity equation:

$$\frac{\partial u_i}{\partial x_i} = 0$$

Here u_i are the mean (phase resolved) velocities, x_i are the Cartesian coordinates, p is the pressure, ν is the kinematic viscosity of water,

$$\frac{\tau_{ij}}{\rho} = \nu_T\left(\frac{\partial u_i}{\partial x_j} + \frac{\partial u_j}{\partial x_i}\right) - \frac{2}{3}k_T\delta_{ij}$$

is the Reynolds stress tensor, expressing the additional shear stresses due to momentum transfer from turbulent fluctuations, and F_{Bi} represent body forces used to drive the flow. δ_{ij} in the equation above is the Kronecker delta,

$$k_T = \frac{1}{2}\overline{u_i' u_i'}$$

is the turbulent kinetic energy (per unit mass), where the overbar denotes time averaging, and

$$\nu_T = \frac{a_1 k_T}{\max(a_1 \omega_T, SF_2)}$$

is the eddy viscosity, where ω_T is the specific dissipation rate of the turbulence. S is the invariant measure of the strain rate and F_2 is the second blending function in the standard two-equation SST (Shear Stress Transport) k-omega turbulence model with standard tuning coefficients.

The above equations are solved in two or three dimensions, subject to the following boundary conditions. The cylinder surface is considered a friction wall, and no-slip boundary conditions are imposed, i.e. all velocity variables are set to zero or to the rotational speed (ωR) at the surface of the cylinder. Velocities at the inlet and outlet are imposed zero gradient boundary conditions. The turbulent kinetic energy, k_T, is imposed zero gradient boundary conditions except at the inlet boundary. Here a fixed value is imposed to specify the turbulence in the incoming flow. Wall roughness on the cylinder is handled with standard wall function for ν_T and ω_T.

The equations are solved using a PISO algorithm, and the resulting Poisson equation for pressure is solved with zero gradient condition at the cylinder wall and a fixed total pressure at the inlet and outlet ($p_0 = p + \frac{1}{2}\rho|\mathbf{u}|^2 = 0$), see /13/. Within the model computational cells are stretched in the radial direction to provide adequate resolution of the boundary layer forming on the cylinder.

The flow is driven with an oscillatory body force, F_B, in the x-direction ($i = 1$).

$$F_B = F_{B0} + \sum_{n=1}^{N} 2\pi f_n U_n \cos(2\pi f_n t + \varphi_n)$$

where t is time. U_n is the free stream velocity amplitude, $f_n = 1/T_n$ is the wave frequency (T_n is the wave period) and φ_n is the phase lag of the nth wave component. F_{B0} is a global forcing term allowing a non-zero mean flow. Only one wave component was used in the present numerical runs.

3.1.1 Geometry

Figure 3.1 shows the basis computational grid in plan view (2D). The computational grid is defined by an inner and an outer radius, R_{in} and R_{out}, respectively. The number of computational cells is the number of discrete cells in the radial direction, N_r, times the number of discrete cells in the angular (azimuth) direction, N_θ. For the basis grid shown in Figure 3.1 the number of cells is $N = N_r \cdot N_\theta = 152 \cdot 360 = 54720$.

The computational cells are stretched in the radial direction to provide adequate resolution of the boundary layer forming on the cylinder. The stretching is defined by:

$$\frac{\Delta r_{n+1}}{\Delta r_n} = \beta$$

where n indicates the nth cell in the radial direction and the height of the nth cell is given by:

$$\Delta r_n = \frac{R_{out} - R_{in}}{\sum_{i=1}^{N_r} \beta^{i-1}} \cdot \beta^n$$

The progression, β, is 1.03 for the basis grid and results in a height to width ratio of approximately 1:5 and 2:1 for the first and final cell in the radial direction, respectively. Figure 3.2 shows a close-up of the basis computational grid close to the cylinder surface, which reveals the height to width ratio.
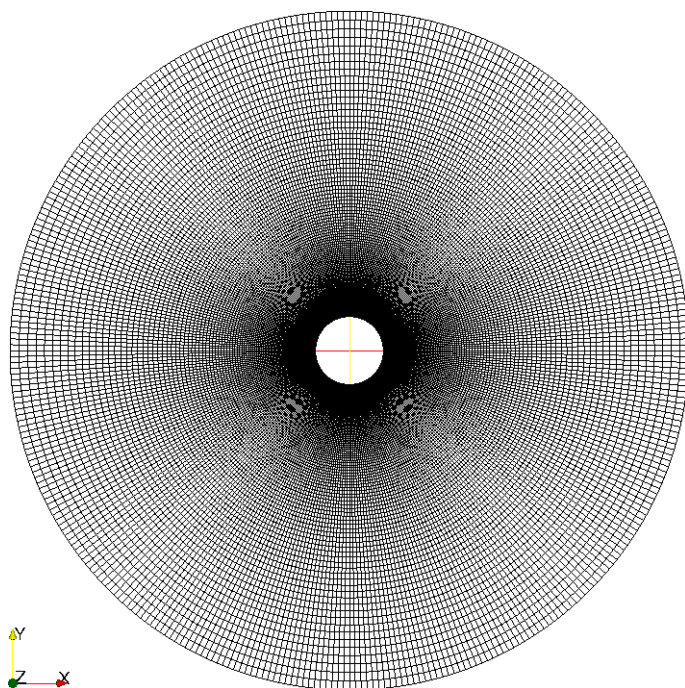
Figure 3.1   Plan view of computational grid (2D). Number of cells: $N = N_r \cdot N_\theta = 152 \cdot 360 = 54720$.
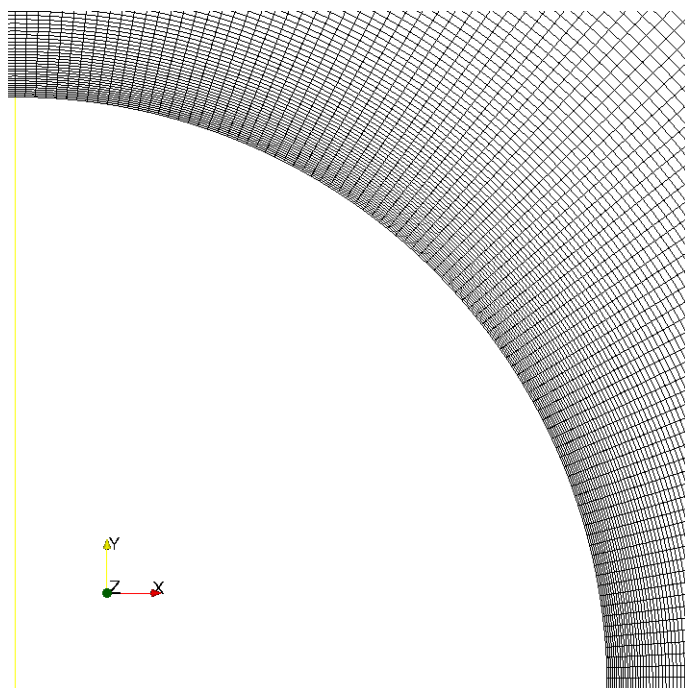

Figure 3.2   Close-up of computational grid (Figure 3.1) at the cylinder surface. Cells are stretched in the radial direction with a progression of $\beta = 1.03$.

3.2 Model Validation

An initial model validation has been performed by comparing the results from the numerical model to published experimental results, independently testing the hydrodynamic effects of rotation, waves and currents on cylinders. Note that the numerical model is essentially similar to that described and validated in /8/ (Furhman *et al.* 2009). For definitions, see e.g. Sections 4 and 5 or a standard textbook.

3.2.1 Steady Current

Figure 3.3 and Figure 3.4 show published experimental drag force coefficients and Strouhal numbers with corresponding results from the numerical model. Blockage correction should be applied to the experimental results, /2/ (Achenback & Heiniche 1981). The blockage correction amounts to D/B = 1/6 = 16.67% where B is the width of experimental facility (air duct). A sound agreement between the published experimental results and the numerical model can be observed from both figures when blockage correction is taken into account.
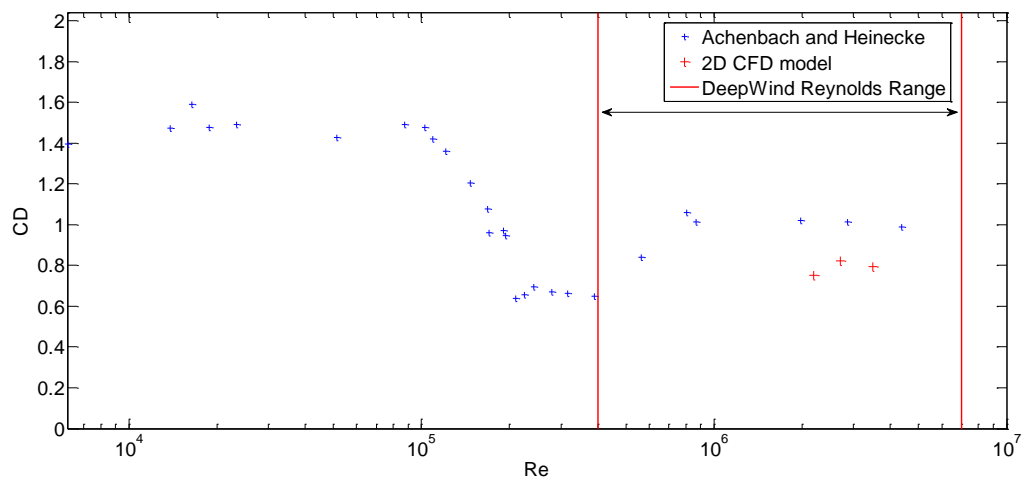
Figure 3.3   Plot of the drag coefficients for a cylinder of roughness ($k_s/D=0.75 \cdot 10^{-3}$), where k_s is the Nikuradse roughness and D is the diameter of the cylinder (Achenbach & Heinecke 1981), as a function of Reynolds number (Re). The CFD model results show sound agreement.

Figure 3.4   Data of Strouhal numbers for a smooth cylinder as a function of Reynolds number (Re), taken from /3/ (Schewe 1983). The CFD model results are from a cylinder with roughness ($k_s/D=0.75 \cdot 10^{-3}$), as presented in the previous figure. Model results are well within the range of experimental points.

3.2.2 Wave alone

Figure 3.5 plots the drag coefficients for a smooth cylinder exposed to an oscillating flow from /4/ (Sarpkaya 1986) and the nu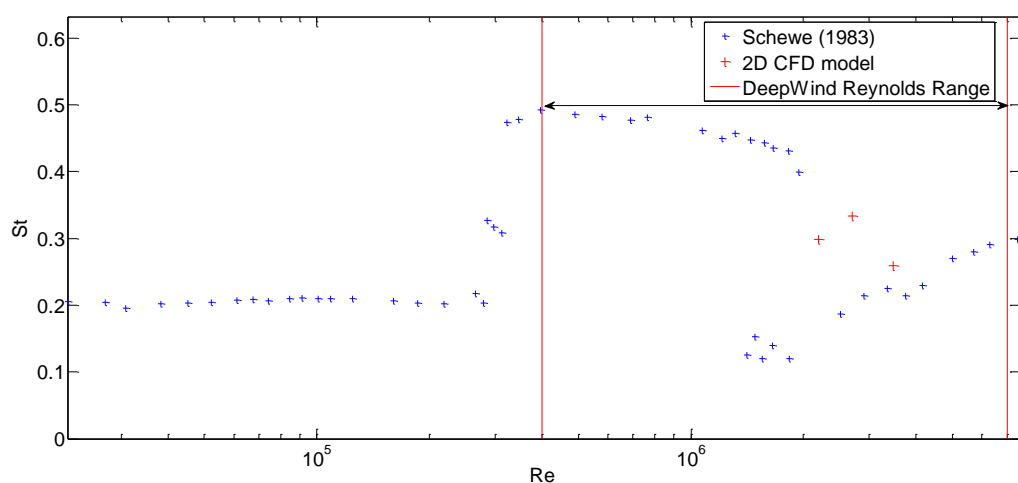merical model. Figure 3.6 plots the corresponding inertia coefficients. The ratio of Reynolds number to Keulegan-Carpenter number is set to 1035 for Figure 3.5 and Figure 3.6.
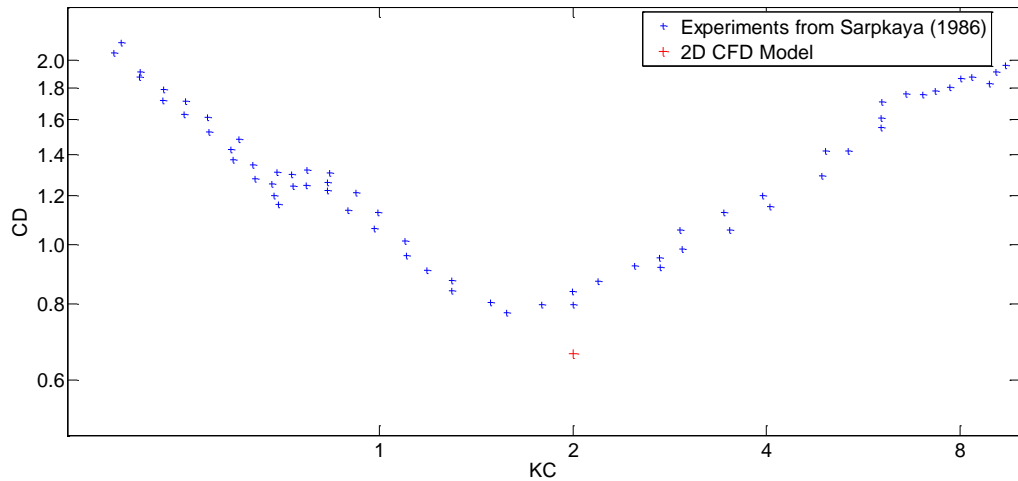
Figure 3.5   Drag coefficients plotted as a function of the Keulegan-Carpenter (KC) number. Re/KC=1035. Experiments from /4/ (Sarpkaya 1986).
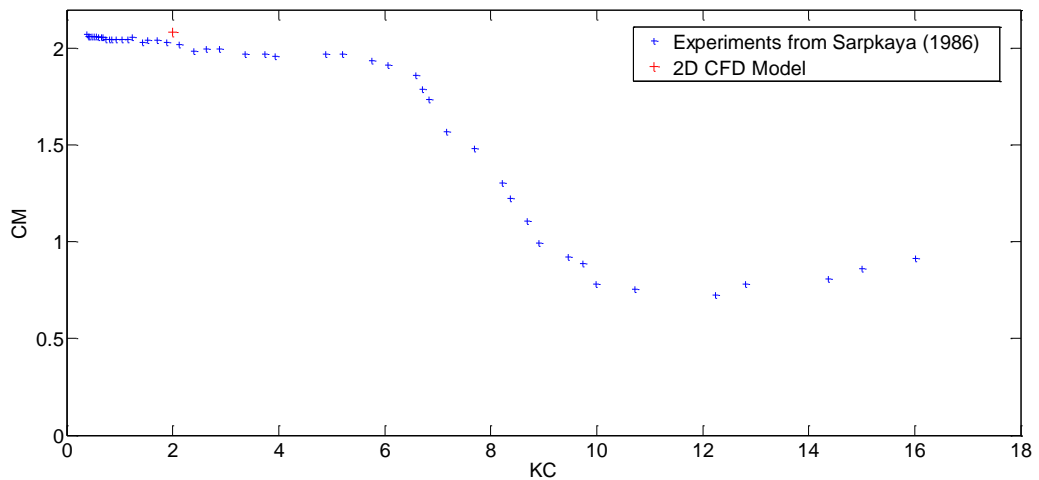
Figure 3.6   Inertia coefficients plotted as a function of the Keulegan-Carpenter (KC) number. Re/KC=1035. Experiments from /4/ (Sarpkaya 1986).

Figure 3.7 plots drag coefficients (C_D) of a rough cylinder in oscillating flow, /5/ (Sarpkaya 1976) with results derived from the numerical model. Figure 3.8 plots the corresponding inertial coefficients (C_M). Sound agreement can be observed for the experimentally and numerically derived inertia and drag coefficients in both Figure 3.7 and Figure 3.8.
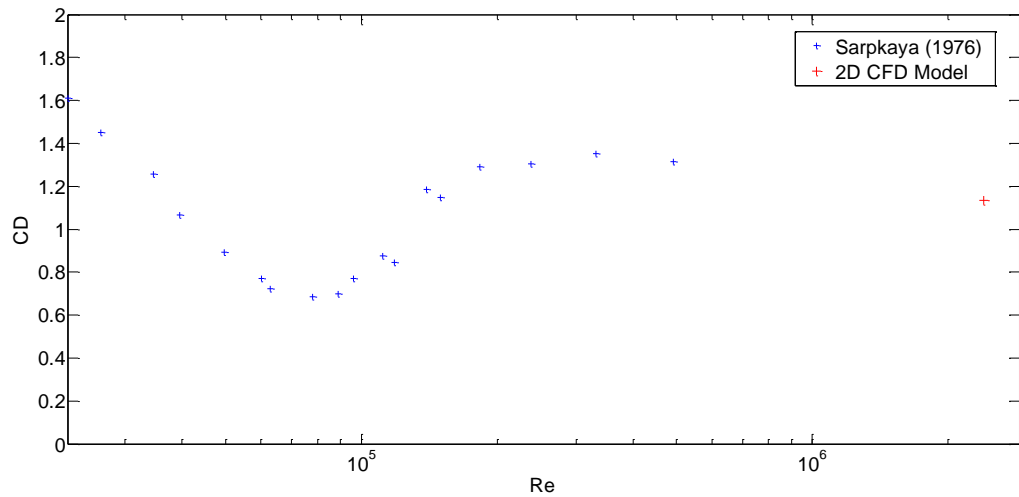
Figure 3.7   *Drag coefficient (C_D) as a function of Reynolds number (Re) for a rough cylinder (k/D =1.25 x 10^{-3}) for KC=20. (Sarpkaya 1976).*

Figure 3.8   *Inertia coefficient C_M (=C_m+1) as a function of Reynolds number (Re) for a rough cylinder (k/D =1.25 · 10^{-3}) for KC=20. (Sarpkaya 1976).*

3.2.3   Rotation alone

Figure 3.9 plots both moment coefficients (C_f) for rough rotating cylinders taken from experiments outlined in /6/ (Theodorsen and Regier 1945) and the numerical model.
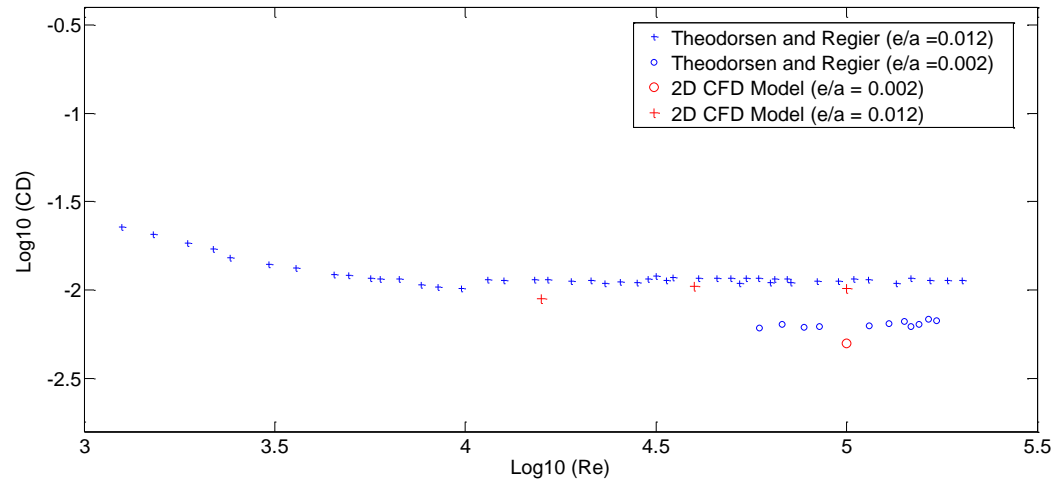
Figure 3.9   Friction coefficient plotted as a function of Reynolds number for a rotating cylinder, for e/a=0.012 and e/a=0.002 where e is the size of the sand used for roughness and a is the radius of the cylinder. (Theodorsen & Regier).

4 TEST CONDITIONS

4.1 Current alone

A few validation runs were performed with steady current: the current speed was in the range U_c = 0.35 ~ 0.60 m/s. The current Reynolds number, defined:

$$Re_c = \frac{DU_c}{\nu}$$

was in the supercritical range. Here ν is the kinematic viscosity (0.01 cm^2 s^{-1}). A total of 4 tests were performed. Additional details regarding the test conditions are given in Appendix A.

4.2 Waves alone

Table 4.1 and Table A.2 (Appendix A) summarize the test conditions for wave alone runs. Note that U_m in the table is the amplitude of the free-stream velocity defined by:

$$U = U_m\sin(2\pi ft)$$

where f = 1/T is the wave frequency (T is the period of the oscillatory motion). The amplitude of the orbital motion is calculated from:

$$a = \frac{U_mT}{2\pi}$$

The Keulegan-Carpenter number and the Reynolds number, respectively, are defined:

$$KC = \frac{2\pi a}{D} = \frac{U_mT}{D}$$

$$Re = \frac{aU_m}{\nu} = \frac{TU_m^2}{2\pi\nu}$$

where ν is the kinematic viscosity (0.01 cm^2 s^{-1}).

The wave alone experiments covered KC numbers in the range 0.3 < KC < 10. A total of 14 tests were performed.

Table 4.1   Test conditions: oscillatory flow (wave) alone; Cylinder diameter, D = 6 m

U_m	T	a	KC	Re · 10^{-6}	N
(m/s)	(s)	(m)	(-)	(-)	(-)
0.6 ~3.6	2.8 ~ 17.4	0.3 ~ 10	0.3 ~ 10	3.5 ~ 21	14

4.3 Rotation alone

A number of validation runs were performed with rotation alone: the rotational frequency was $\omega/2\pi = 0.02$ to 0.1 rpm. Re_ω is the Reynolds number based on the surface speed:

$$Re_\omega = \frac{\omega R^2}{\nu}$$

was in the range $4 < \log_{10}(Re_\omega) < 5$. Here ωR is the surface speed of the cylinder. Additional details regarding the test conditions are given in Appendix A.

4.4 Current with Rotation

A number of validation runs were performed with steady current and cylinder rotation: the current speed was $U_c \approx 0.60$ m/s; and the cylinder rotation was in the range $\omega/2\pi = 0 \sim 6$ rpm. The current Reynolds number was in the supercritical range: $3.6 \cdot 10^6$; and the speed ratio, $\omega R/U_c$, was between 0 and 4. Additional details regarding the test conditions are given in Appendix A.

4.5 Wave with Rotation

Table 4.2 summarizes the test conditions for wave with rotation runs.

The cylinder rotation may be expressed as the ratio of surface speed and the free stream velocity (the speed ratio):

$$\alpha = \frac{\omega D}{2U_m} = \frac{\omega R}{U_m}$$

Here R is the cylinder radius and ω is the angular frequency of the cylinder. In Table 4.2 the range of angular frequency tested has been indicated.

A total of 17 runs were performed. Additional details regarding the test conditions are given in Appendix A.

Table 4.2   Test conditions: oscillatory flow with cylinder rotation; Cylinder diameter, D = 6 m

U_m	T	a	KC	$Re \cdot 10^{-6}$	$\omega/2\pi$	N
(m/s)	(s)	(m)	(-)	(-)	(rpm)	(-)
2.25	11.0	4.0	4.1	14	0 ~ 15	4
1.95	9.6	3.0	3.1	12	15 ~ 30	3
1.59	7.8	2.0	2.1	9.7	15 ~ 30	2
1.13	5.5	1.0	1.0	6.8	15 ~ 20	2
0.80	3.9	0.5	0.5	4.8	15	1
2.0 ~3.0	11.0	3.5 ~ 5.3	3.5 ~ 5.5	12 ~ 18	15	3
3.0	12.0	5.7	5.9	18	20	1
2.25	8	2.9	3.0	14	10	1

4.6   *Combined Wave and Current with Rotation*

Table 4.3 summarizes the test conditions for combined wave and current with rotation experiments. A total of 41 runs were performed. Additional details regarding the test conditions are given in Appendix A.

Table 4.3   Test conditions: combined wave and current with cylinder rotation; Cylinder diameter, D = 6 m.

U_m	T	a	KC	U_c	$|V_c|$	$\omega/2\pi$	$\omega R/(U_m+U_c)$	N
(m/s)	(s)	(m)	(-)	(m/s)	(m/s)	(rpm)	(-)	(-)
2.25	11.0	4.0	4.1	0.1 ~ 0.5	0.0 ~ 0.3	5 ~ 15	0.7 ~ 2.0	7
1.97	9.6	3.0	3.1	0.0 ~ 0.6	0.0 ~ 0.3	5 ~ 20	0.7 ~ 3.1	13
1.61	7.8	2.0	2.1	0.1 ~ 0.7	0.0 ~ 0.2	5 ~ 15	0.9 ~ 2.8	7
1.14	5.5	1.0	1.0	0.1 ~ 0.6	0.0 ~ 0.5	5 ~ 25	1.2 ~ 6.4	14

5 RESULTS

5.1 Force Formulation

5.1.1 In-line Force

For oscillatory flow the total ensemble-averaged in-line force can be formulated as (the Morison formulation):

$$F_x = \frac{1}{2}\rho C_D D U |U| + \rho C_{mX} A \frac{dU}{dt} + \rho A \frac{dU}{dt}$$

where ρ is the fluid density, C_D is the drag coefficient, D is the diameter of the cylinder, C_m is the hydrodynamic mass coefficient, A is the cross-sectional area of the cylinder, and U is the fluid velocity. In the numerical model, however, the Froude-Krylov force, the last term on the right-hand side, is not present and the in-line force formulation becomes:

$$F_x = \frac{1}{2}\rho C_D D U |U| + \rho C_{mX} A \frac{dU}{dt}$$

For co-linear combined oscillatory flow and current the velocity can be taken as:

$$U = U_c + U_w$$

where U_c is the current velocity and U_w is the wave velocity. For an oscillatory flow the wave velocity is given by:

$$U_w = U_m \sin(2\pi f t + \varphi)$$

where U_m is the maximum velocity, $f = 1/T$ is the wave frequency (T is the wave period) and φ is phase lag of the wave.

The Morison formulation is fitted by a least squares method to in-line force exhibited on the cylinder, in order to obtain values for C_D and C_{mX}.

5.1.2 Cross-flow Force

The ensemble-averaged cross-flow (lift) force of a long non-rotating circular cylinder in combined wave and current is zero.

For clock-wise rotating circular cylinder in steady current the velocity of the upper surface of the cylinder is in the same direction as the free-stream velocity. Separation is thereby delayed on the upper surface, whereas it occurs earlier on the lower surface. As a result the pressure distribution on the cylinder surface is altered when the rotation is present. Pressure is reduced on the upper surface and increased on the lower surface, causing a positive net lift force. Rotation in the opposite direction reverses this effect and causes a negative lift force. The lift force can be formulated as:

$$F_Y = \frac{1}{2}\rho C_L D U_c^2$$

where C_L is the lift coefficient.

For co-linear combined wave and current the lift force can, as detailed in /7/, be formulated as:

$$KC \lesssim 10: \qquad F_Y = \rho C_\Gamma A \omega U + \rho A C_{mY} \frac{dU}{dt}$$

$$KC \gtrsim 10: \qquad F_Y = \frac{1}{2} \rho C_L D U |U| + \rho A C_{mY} \frac{dU}{dt}$$

where C_Γ is the Kutta-Joukowski coefficient and C_{mY} is the hydrodynamic mass coefficient in the transverse direction. The lift formulation for the steady current is seen to be a special case of the general formulation above as $KC \to \infty$.

The formulation is fitted by a least squares method to the measured cross-flow forces in order to obtain values for C_L and C_{mY}.

5.2   Current alone

The current alone case was partially treated under the model validation (Section 3.2.1). Figure 5.1 shows the measured drag coefficient in the present experiments. Also shown in the figure is a general form of $C_D = C_D(Re_c, k_s/D)$ for $k_s/D = 1.5 \cdot 10^{-6}$ (smooth) through $k_s/D = 3 \cdot 10^{-3}$ from /9/. As for the physical model experiments there is good comparison between the present results and the general form of $C_D = C_D(Re_c, k_s/D)$ presented in /9/.
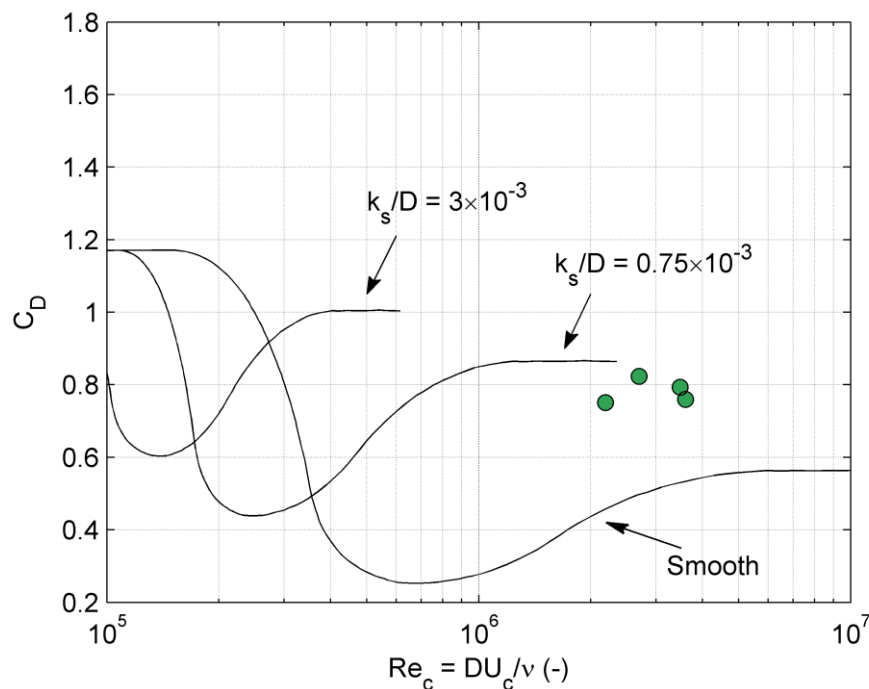

Figure 5.1   *Drag coefficient of a circular cylinder at various surface roughness parameters, k_s/D, as a function of the Reynolds number. Filled circles: present data; Curves: general form of $C_D = C_D(Re_c, k_s/D)$ curve for a rough cylinder (Basu (1985) /9/) for $k_s/D = 1.5 \cdot 10^{-6}$ (smooth), $0.75 \cdot 10^{-3}$, $3 \cdot 10^{-3}$.*

5.3   Wave alone

The wave alone case was partially treated under the model validation (Section 3.2.2).

For reference a number of runs with wave alone were performed. In all runs the KC number was less than approximately 10 with realistic full-scale wave period and amplitude. For each run the drag and inertia coefficients were determined using the least-squares method. Figure 5.2 shows the determined drag and inertia coefficients.
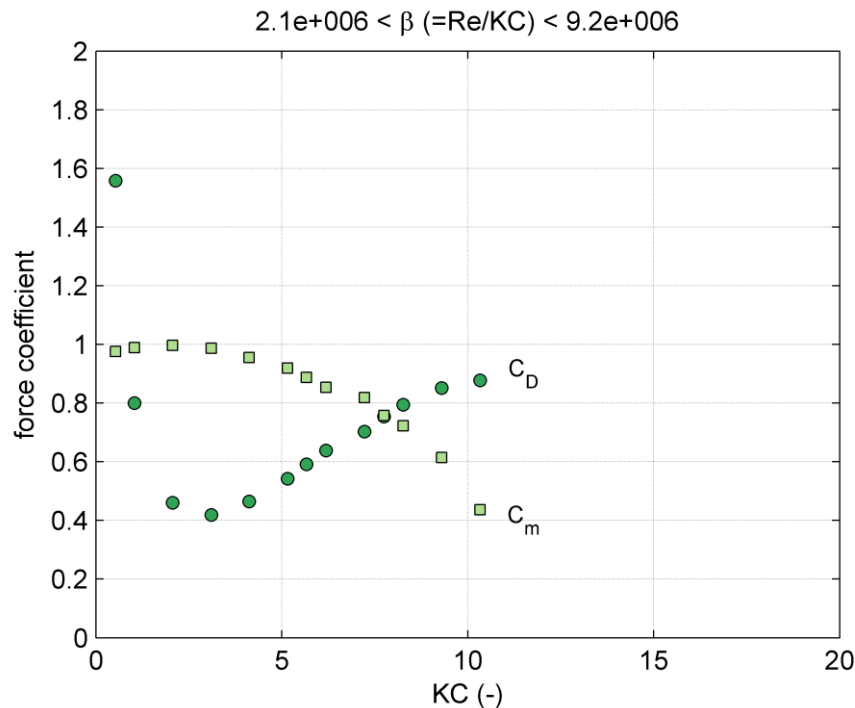
Figure 5.2   Drag and inertia coefficients versus Keulegan-Carpenter number.

5.4   Rotation alone

The rotation alone case was treated under the model validation (Section 3.2.3).

The friction torque, M_z (moment) may be represented by the non-dimensional friction coefficient:

$$C_f = \frac{M_Z}{\frac{1}{2}\rho SR(\omega R)^2}$$

where S (=2πRh) is the surface area of the cylinder, ωR is the surface speed of the cylinder, and the quantity ½ρ(ωR)^2 is the dynamic pressure associated with the surface speed.

Figure 3.9 shows the modelled friction coefficient as a function of Re_ω. Recall that Re_ω is the Reynolds number based on the surface speed:

$$Re_\omega = \frac{\omega R^2}{\nu}$$

Also plotted in the figure are data from Theodorsen & Kegier (1945) /6/. Generally, the at present measured drag coefficients are of the same order of magnitude as those reported by Theodorsen & Kegier – although slightly smaller assuming that the present relative roughness, d_{50}/R, corresponds to the relative roughness, ε/R, reported by Theodorsen & Kegier). See /7/ for further discussion of this.

5.5   Current with Rotation

Figure 5.3 shows the measured lift and drag coefficient as a function of the speed ratio, $\omega R/U_c$, the ratio of surface speed to free-stream flow speed. In Figure 5.3 experimentally measured lift and drag coefficients for subcritical Reynolds numbers between 40 000 and 660 000 from /10/ have also been included. The Reynolds numbers in the CFD model are in the supercritical range so a direct comparison with the experimental results reported in /10/ is not sound. However, the lift and drag coefficients show the expected behaviour.
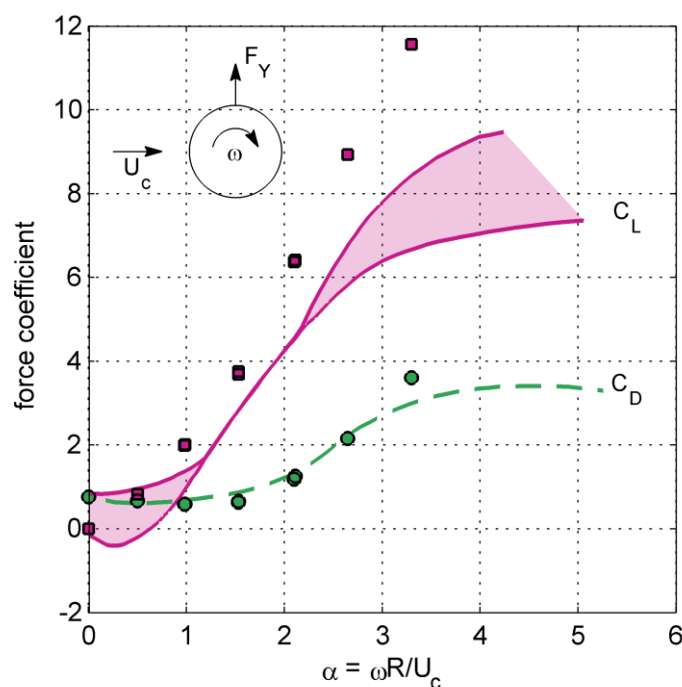

Figure 5.3   *Lift and drag of a rotating cylinder as a function of speed ratio: Magnus force. Circles and squares: present data; lines: /10/.*

Potential flow theory predicts zero drag force ($C_D = 0$) and a lift force given by:

$$F_Y = \rho \Gamma U_c = \rho(2\pi\omega R^2)U_c$$

the *Kutta-Joukowski theorem*. Hence, potential flow theory predicts a lift coefficient given by:

$$C_L = \frac{\rho(2\pi\omega R^2)U_c}{\rho R U_c^2} = 2\pi\frac{\omega R}{U_c} = 2\pi\alpha$$

This theoretical value is higher than CFD model results suggest, a discrepancy that is primarily due to viscosity. However, the measured variation of C_L with respect to the speed ratio is to some extent in accordance with the theoretically predicted linear variation.

5.6 Wave with Rotation

Figure 5.6 shows the ensemble-averaged in-line and cross-flow force at different KC numbers. Also included in the graphs are the measured velocity and acceleration. The graphs show that the cross-flow force variation is similar to the velocity for KC < 6.

There is a small phase shift between the velocity and the cross-flow force indicating a contribution from inertia as argued for in Section 5.1.2 (see also /7/). The test conditions (Section 4) show that there are only tests with KC < 5. From the results presented in /7/ it is expected that there is a change from one flow regime to another somewhere in the range 8.2 < KC < 12.5 where the limit KC ≡ 10 between the two regimes is regarded as a best guess based on the results in /7/. Interestingly, the KC number range, 8.2 < KC < 12.5, coincides with the transverse vortex-street regime (7 < KC < 13) and the start of vortex shedding (KC > 7) in pure oscillatory flow around a non-rotating cylinder, see /11/.

The lift (or Kutta-Joukowski) and inertia coefficient has been determined using the method of least squares:

For **KC < 10** the formulation with C_Γ has been used. Figure 5.4 shows the lift, expressed with C_Γ and C_{mY}, as a function of the relative rotational speed. C_Γ is in the order of 1 when $\omega R/U_m = 1.5$. It gradually decreases with increasing speed ratio and appears to approach the value 0.5 asymptotically for $\omega R/U_m > 4$. A value that is substantially smaller than the potential flow solution, $C_\Gamma \equiv 2$. Even at small speed ratios, such as $\omega R/U_m = 0.5$, the measured C_Γ is somewhat smaller than the value predicted by the potential flow solution. For $\omega R/U_m < 0.5$ the Kutta-Joukowski coefficient is expected to increase with decreasing speed ratio, although with an upper limit given by the potential flow solution, $C_\Gamma \equiv 2$. The inertia coefficient, C_{mY}, appears to attain a constant value of 0.2 over the entire range of speed ratios tested ($0.5 < \omega R/U_m < 6$), if the scatter in the data points is neglected. Figure 5.6 includes the predicted cross-flow force. The predicted cross-flow force is calculated from the determined force coefficients using the cross-flow force formulation. The figure shows a good agreement between the measured and predicted cross-flow force.

The Kutta-Joukowski coefficient, C_Γ, (Figure 5.4) has been recalculated to a lift coefficient, C_L. The corresponding lift coefficient is shown in Figure 5.5. The lift coefficient is a function of the relative rotational speed. For oscillatory flow around a rotating cylinder, the lift coefficient, C_L, is approximately 5 at the speed ratio, $\omega R/U_m = 2$ (Figure 5.5). This is almost the same value as the CFD model predicts for steady flow around a rotating cylinder (see Figure 5.3). For $\omega R/U_m < 2$ the lift coefficient in the unsteady case is higher than in the steady case. And for $\omega R/U_m > 2$ the lift coefficient is smaller in the

unsteady case than in the steady case. In the steady case for an ideal fluid, $\omega R/U_c = 2$, corresponds to the instance when the two stagnation points coincide to form a single stagnation point at the bottom of the cylinder surface. Above this value the single stagnation point will move off into the fluid as either a single stagnation point or two stagnation points. This may possibly be related to the observed difference between the unsteady and steady case.
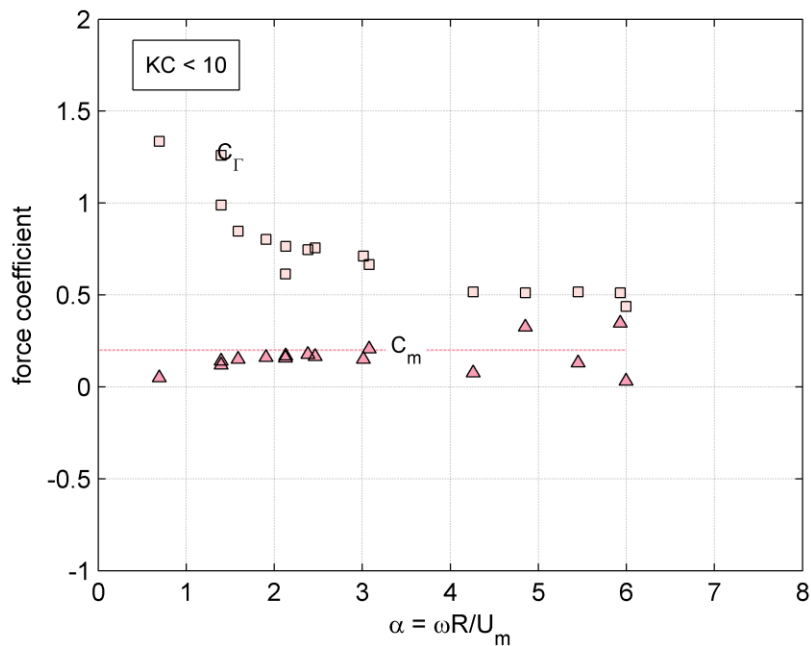
Figure 5.4   Lift, expressed with C_Γ and C_m, of a rotating cylinder in waves as a function of relative rotational speed (KC < 10). Dotted line: average value for the inertia coefficient, C_m.
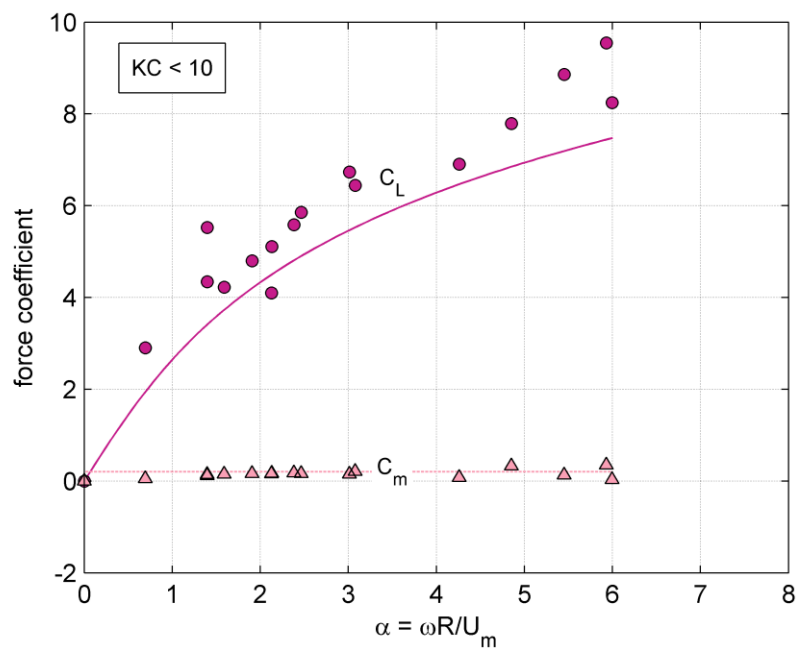
Figure 5.5   Lift of a rotating cylinder in waves as a function of relative rotational speed (KC < 10). Solid line: best fit to experimental data (C_L) in /7/. Dotted line: average value for the inertia coefficient, C_m.
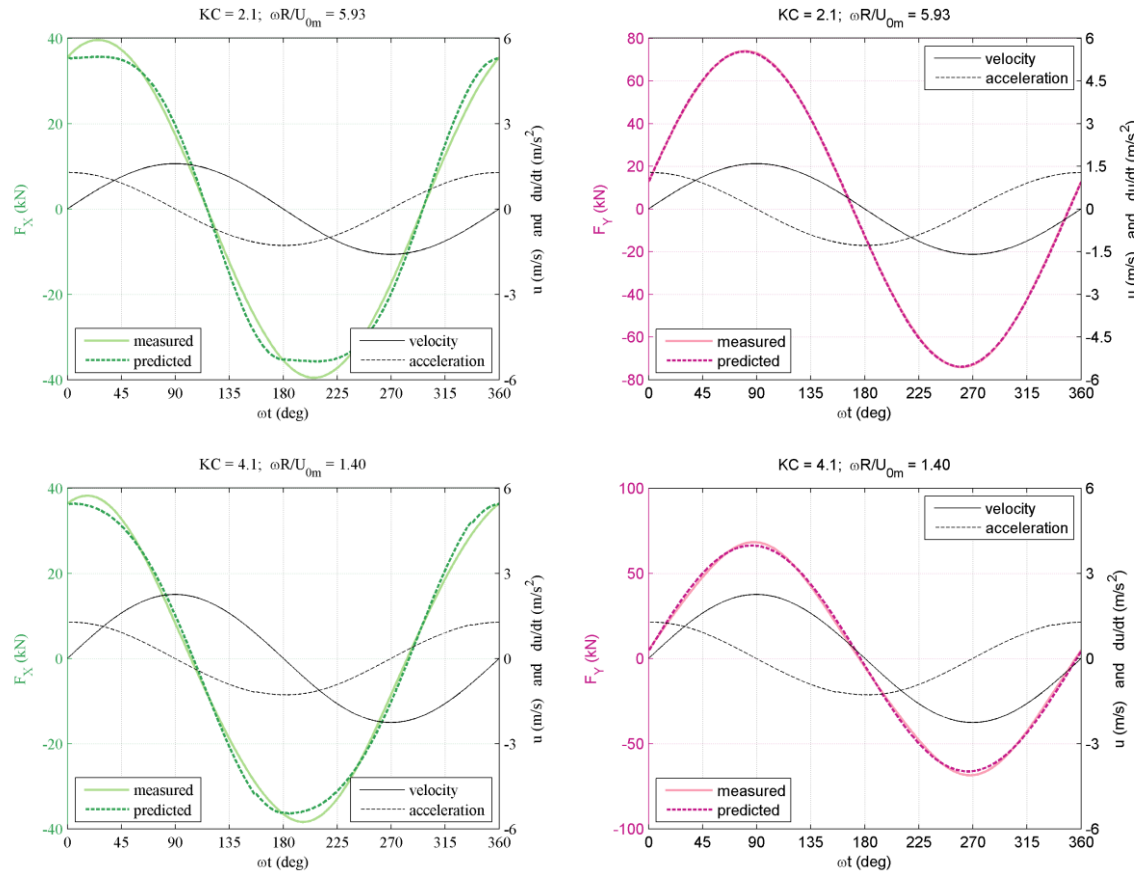
Figure 5.6   Comparison of measured and predicted in-line and cross-flow force: (a) KC = 2.1, and (b) KC = 4.1. Run No. 83.19 and 83.15, respectively.

The in-line force is determined as for the wave alone case, see Sections 5.1.1 and 5.3. Figure 5.7 shows the measured in-line force expressed as a drag and inertia coefficient (hydrodynamic mass coefficient). The force coefficients are expressed as a ratio to the force coefficients in the wave alone case. The number of data points is small. There is, however, an indication that the cylinder rotation, i.e. the Magnus effect, could be affecting the in-line drag force. The trend has been indicated in the figure. The in-line hydrodynamic mass force appears not to be affected by cylinder rotation.
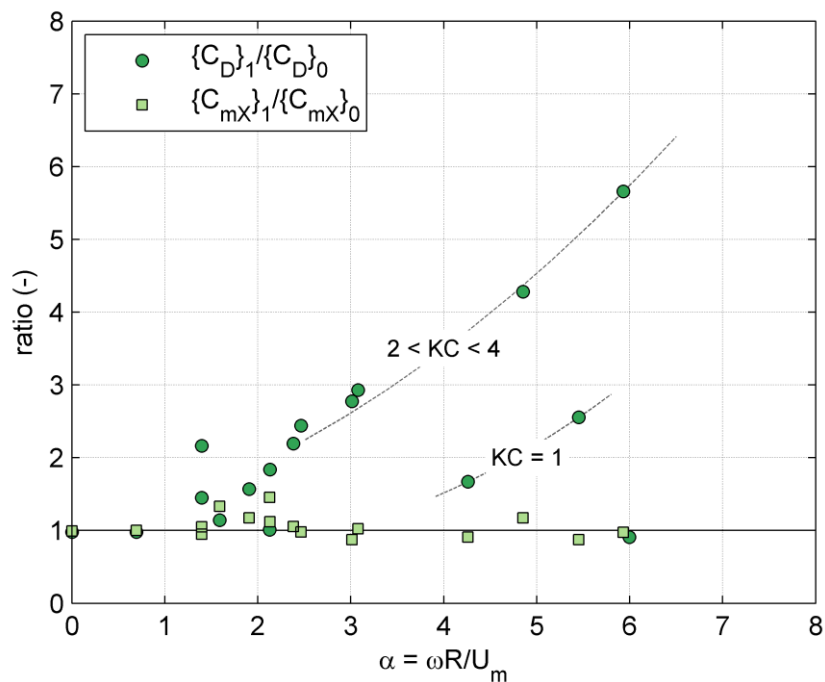
Figure 5.7   Variation of C_D and C_{mX} with KC number for the case wave with rotation. Indices 1 and 0 represent with and without cylinder rotation, respectively. (E.g. $\{C_D\}_0$ is the drag coefficient in waves alone, Figure 5.2). The results should not be extrapolated to higher KC number without supplementary modelling or experiments.

5.6.1   Friction Torque

The average friction torque, M_z (moment) may be represented by the non-dimensional friction coefficient as detailed in Section 5.4. Figure 5.8 shows the measured friction coefficient as a function of Re_ω. Also plotted in the figure are data from Theodorsen & Kegier (1945) /6/. Generally, the drag coefficients for the wave with rotation case are of the same order of magnitude as those for rotation alone.
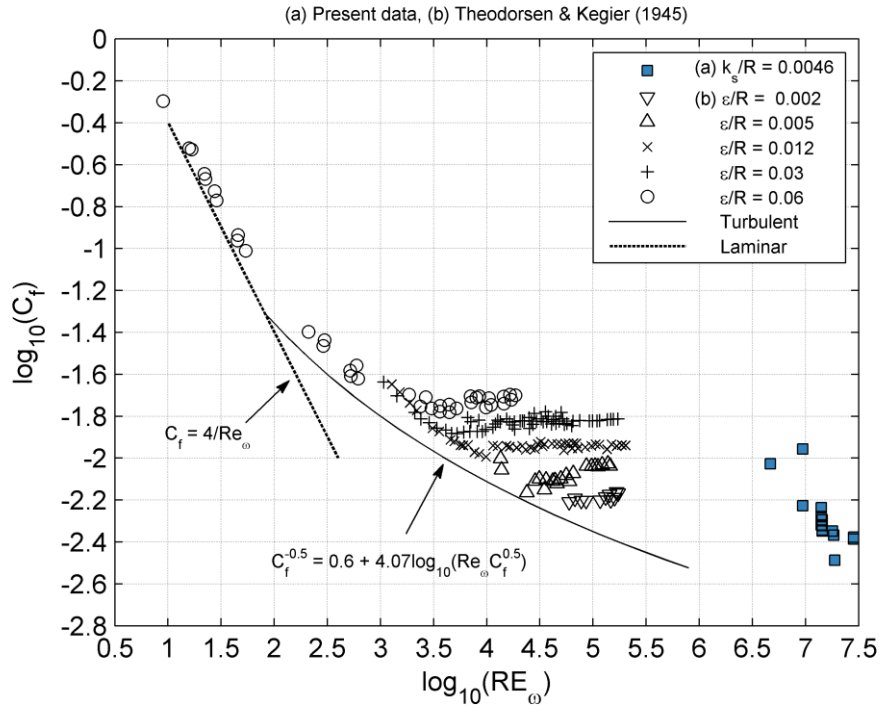
Figure 5.8   *Friction coefficient, C_f, as a function of Re_ω. (a) Solid squares: present data; (b) Other data from Theodorsen & Kegier (1945) /6/. Dotted line: smooth surface, laminar flow. Solid line: smooth surface, turbulent flow.*

5.6.2   *In-line Versus Cross-flow Force*

Figure 5.9 shows the in-line force (inclusive of the Froude-Krylov force) versus the cross-flow force. The figure shows that the in-line force is generally larger than the cross-flow force for KC < 6. The lift force is in the order of (0.5 to 2 times) the in-line hydrodynamic mass force (in-line force without the Froude-Krylov force).

For KC < 6 the maximum in-line and cross-flow force can be written as:

$$\max\{|F_X|\} \approx \max\left\{\rho A h C_M \frac{dU}{dt}\right\} = \rho A h C_M \frac{2\pi}{T} U_m$$

$$\max\{|F_Y|\} \approx \max\{\rho A h C_\Gamma \omega U\} = \rho A h C_\Gamma \omega U_m$$

respectively, when the Froude-Krylov force has been considered in the in-line force, i.e. $C_M = C_m + 1$. Recall that ω is the angular frequency of the cylinder rotation, and $f = 1/T$ is the wave frequency (the inverse of the wave period); and note that there is approximately a 90 degree phase difference between the maximum in-line force and the maximum cross-flow force. The ratio between the maximum cross-flow force and the maximum in-line force then reads:

$$\frac{max\{|F_Y|\}}{max\{|F_X|\}} \approx \frac{\rho A h C_\Gamma \omega U_m}{\rho A h C_M \frac{2\pi}{T} U_m} = \frac{C_\Gamma}{C_M} \frac{\omega T}{2\pi}$$

which says that if U_m and T are kept constant (which means that KC is constant and C_M is constant) then the maximum cross-flow force will increase with ω given the weak

variation of C_Γ with ω (Figure 5.4 with fixed U_m). Furthermore, for small KC numbers (KC < 5) the force ratio will be a function of C_Γ when keeping ω and T constant where $C_M = 2$. Given the weak variation of C_Γ with U_m (Figure 5.4 with fixed ω) especially for $\omega R/U_m > 2$ there will be an almost constant ratio between the maximum in-line and cross-flow force. The two situations have been illustrated in Figure 5.9. Generally, the force ratio is difficult to describe with the non-dimensional parameters, KC and $\omega R/U_m$.

These results are identical to the experimental results, see /7/.
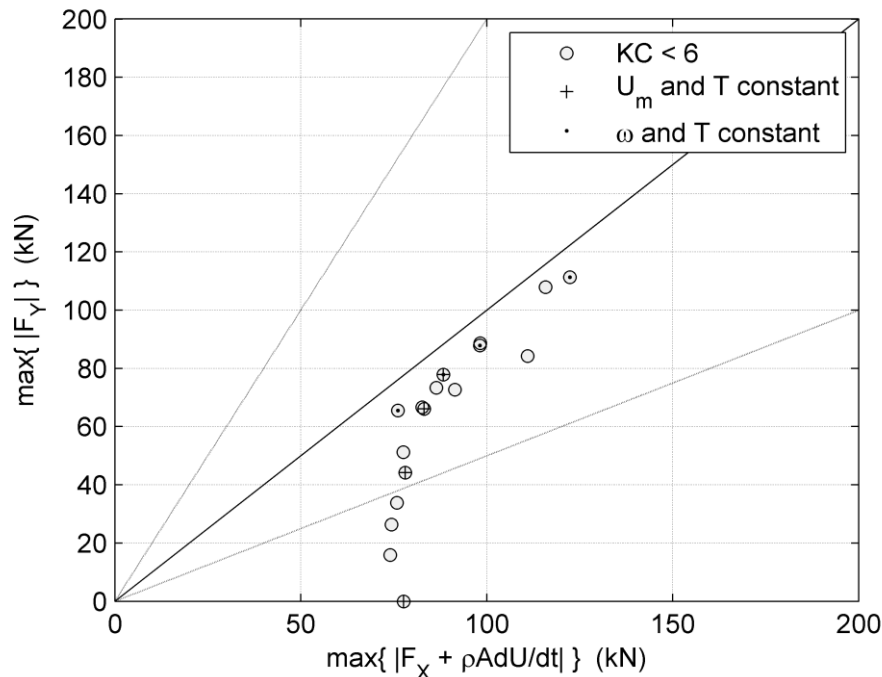
Figure 5.9   In-line (incl. Froude-Krylov force, $\rho h dU/dt$) versus cross-flow force for the case: wave with rotation.

5.7   *Combined Wave and Current with Rotation*

Figure 5.10 gives the definition sketch for combined oscillatory flow (wave) and current with cylinder rotation. Section 5.1 gives the force formulation for *co-linear* combined wave and current, which was established from the physical model experiments, see /7/. In the physical model experiment only co-linear wave and current was studied. Depending on the wave to current alignment there can be a significant cross-flow component of the current as indicated in Figure 5.10. In the extreme case there is a 90º angle between the wave and the current, i.e. $U_c = 0$. The other extreme is co-linear wave and current, i.e. $V_c = 0$. Combined wave and current with cylinder rotation can be split in other ways than indicated in Figure 5.10. The advantage of the split given in Figure 5.10 is that it builds upon the basic flow cases.
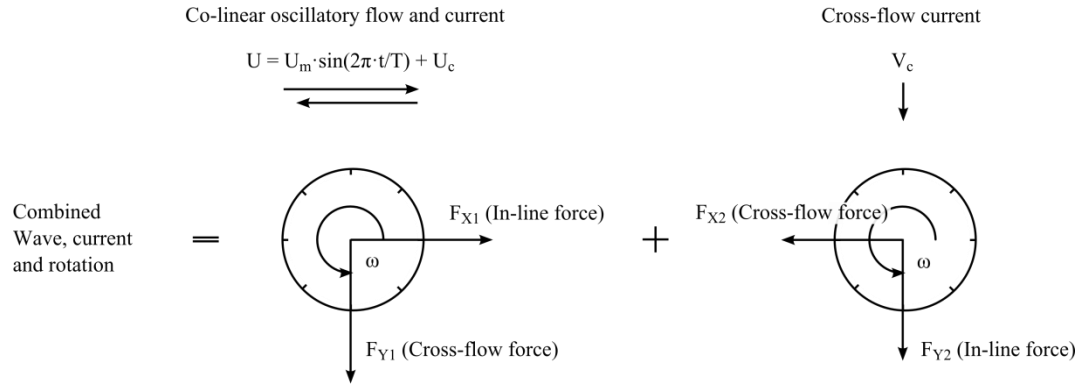
Figure 5.10   *Definition sketch for combined wave and current with cylinder rotation. Note that the sign of the forces may change depending of the cross-flow current and the direction of cylinder rotation.*

Following the definition sketch in Figure 5.10 the formulation for the in-line force in co-linear wave and current (F_{X1}):

$$F_{X1} = \frac{1}{2}\rho C_D D U |U| + \rho C_{mX} A \frac{dU}{dt}$$

may be superposed the cross-flow force of the cross-flow current component (F_{X2}):

$$F_{X2} = \frac{1}{2}\rho C_{L2} D V_c^2$$

to get the total force in the X-direction, which with the direction of the cross-flow current and the direction of the cylinder rotation becomes:

$$F_X = F_{X1} - F_{X2} = \frac{1}{2}\rho C_D D U |U| + \rho C_{mX} A \frac{dU}{dt} - \frac{1}{2}\rho C_{L2} D V_c^2$$

Similarly the total force in the Y-direction **given KC < 10** may be written:

$$F_Y = F_{Y1} + F_{Y2} = \rho C_\Gamma A \omega U + \rho C_{mY} A \frac{dU}{dt} + \frac{1}{2}\rho C_{D2} D V_c^2$$

Note that the sign of the forces may change depending of the direction of the cross-flow current and the direction of the cylinder rotation.

Figure 5.11 shows the ensemble-averaged in-line and cross-flow force at two different KC numbers. Also included in the graphs are the measured velocity and acceleration in the X-direction. The flow situation is as sketched in Figure 5.10. The cross-flow velocity component is in the negative Y-direction and the phase-averaged force in the Y-direction is therefore negative. The phase-averaged force in the X-direction is also negative, which means that the absolute value of the cross-flow force from the cross-flow current component is larger than the in-line force from the in-line current component, i.e. $|\overline{F_{X2}}| > |\overline{F_{X1}}|$. Also included in the figures is the predicted total force in the X- and Y-direction. The predicted total force has been calculated using the formulation above and the determined force coefficients (see below). A good agreement between the predicted and measured total force is noticeable.
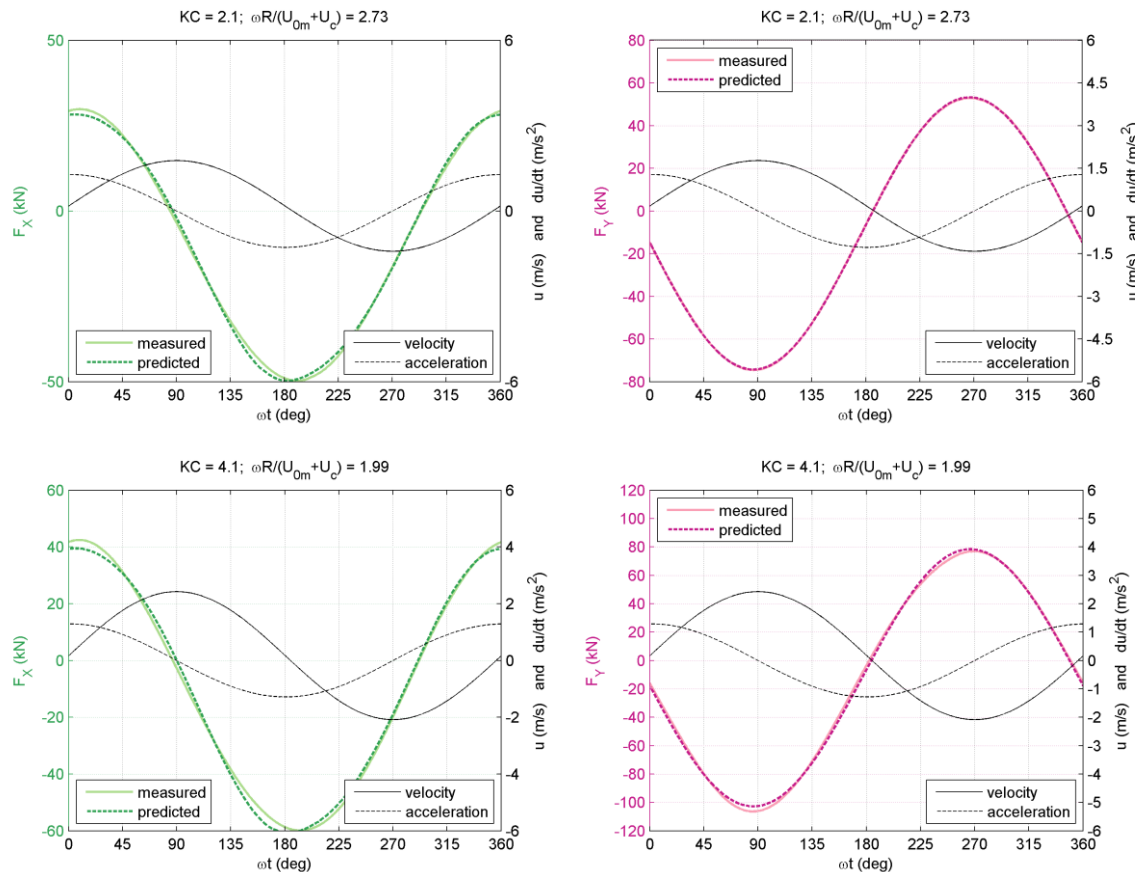
Figure 5.11   Comparison of measured and predicted in-line and cross-flow force: (a) KC = 2.1 [U_m = 1.59 m/s, T = 7.8 s] and (b) KC = 4.1 [U_m = 2.25 m/s, T = 11.0 s]. Run No. 88.5 and 88.7, respectively. U_c = 0.17 m/s and V_c = -0.17 m/s. Cylinder rotating counter-clockwise. See definition sketch in Figure 5.10.

5.7.1   Cross-flow Force Coefficients

Co-linear Wave and Current Component
The cross-flow force coefficients have been determined in an iterative manner: The lift (or Kutta-Joukowski) and inertia coefficients have been determined using the method of least squares with an initial guess for the value of C_{D2} (C_{D2} = 0). Subsequently, C_{D2} has been calculated from the phase-averaged difference between the measured force in the Y-direction and the predicted F_{Y1}. The calculated C_{D2} has then been used as the new guess and the process has been repeated until the calculated force coefficients converged.

Only runs with **KC < 10** have been performed. Figure 5.12 shows the total force in the Y-direction, expressed with C_Γ and C_{mY}, as a function of the relative rotational speed. The force coefficients are comparable to those found for the wave-alone case. This was also the conclusion in the physical model experiments. The Kutta-Joukowski coefficient, C_Γ, (Figure 5.12) has been recalculated to a lift coefficient, C_L. The corresponding lift coefficient is shown in Figure 5.13. When re-calculated to a lift coefficient the scatter in the data points, which is larger than for the wave with rotation case, becomes more apparent.
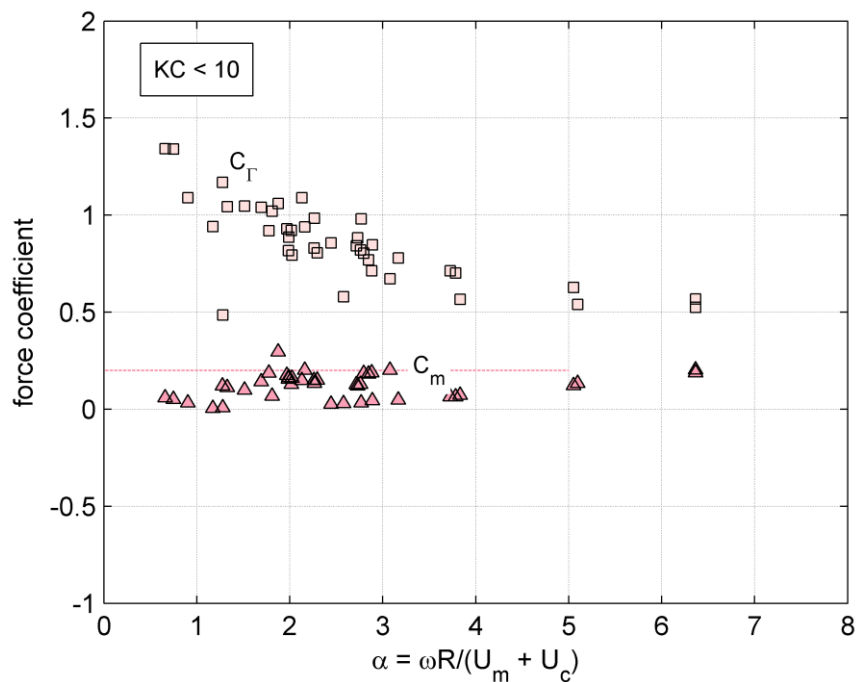
Figure 5.12   Lift, expressed with C_Γ and C_{mY}, of a rotating cylinder in combined wave and current as a function of relative rotational speed (KC < 10). Dotted line: $C_m = 0.2$ as in Figure 5.5.
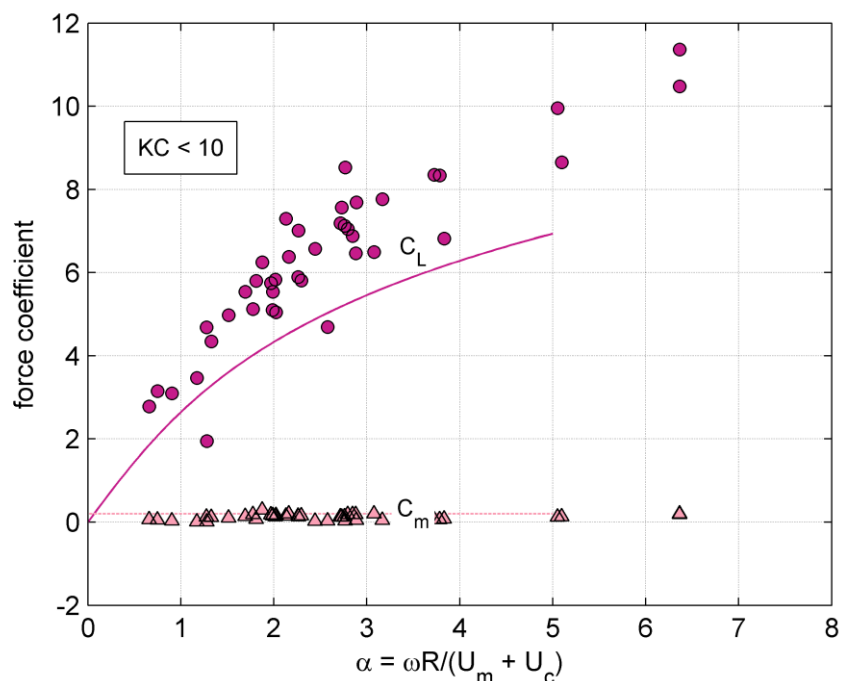
Figure 5.13   Lift of a rotating cylinder in waves as a function of relative rotational speed (KC < 10). Solid line: best fit to experimental data (C_L) in /7/. Dotted line: $C_m = 0.2$ as in Figure 5.5.

Figure 5.14 shows the cross-flow inertia coefficient as a function of the relative wave to current strength. For $U_c/(U_m + U_c) < 0.4$ the cross-flow inertia coefficient scatters between the values 0 and 0.2. No runs were carried out with $U_c/(U_m + U_c) > 0.4$. In the

physical model experiments, /7/, the cross-flow inertia coefficient (the phase lag) reduces while the scatter increases when $U_c/(U_m + U_c)$ increases beyond 0.4. For $U_c/(U_m + U_c) < 0.4$ the numerical model predicts slightly lower inertia coefficient than the physical model experiments, on average 0.1 versus 0.2 in the physical model experiments. The results of the numerical modelling are, however, within the spreading of the results of the physical model experiments.
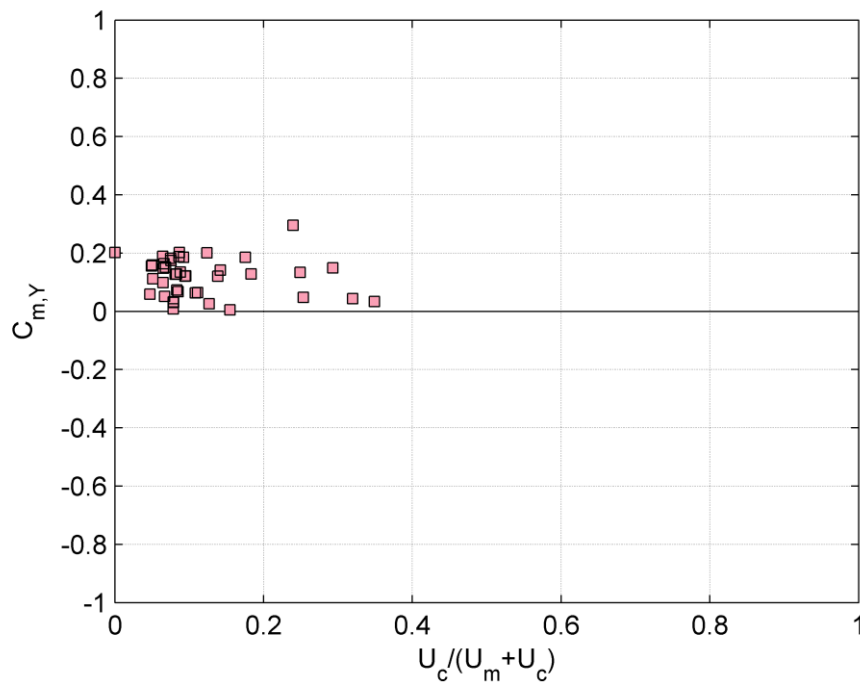
Figure 5.14   Cross-flow inertia coefficient as a function of the relative strength of the wave to current, $U_c/(U_m + U_c)$. KC < 5. $0 < \omega R/(U_m + U_c) < 7$.

Cross-flow Current Component
The lift coefficient, C_{L2}, determined for the cross-flow current component is given in Figure 5.15. The lift coefficient is expressed as a Kutta-Juokowski coefficient:

$$C_{\Gamma 2} = \frac{F_{X2}}{\rho A \omega V_c} = \frac{\frac{1}{2}\rho C_{L2} D V_c^2}{\rho \pi R^2 \omega V_c} = \frac{C_{L2}}{\pi} \frac{V_c}{\omega R} = \frac{C_{L2}}{\pi \alpha}$$

where in potential flow theory $C_{\Gamma 2} \equiv 2$. Recall, as detailed in /7/, that the Magnus lift in potential flow theory is described by the Kutta-Joukowski force, $F = \rho \Gamma V = \rho(2\pi\omega R^2)V \equiv \rho C_\Gamma A \omega V$. Figure 5.15 shows that the determined Kutta-Joukowski coefficient is spread around a constant value. The constant value has been determined to 1.16. This means that the lift coefficient, C_{L2}, is increasing linearly with the speed ratio, α, as potential flow theory predicts. However, the numerical model results suggest that the slope of the linear increase is only $1.16/2 = 60\%$ of that predicted by potential flow theory.

In Figure 5.16 the lift coefficient determined for the cross-flow current component is compared with the lift coefficient determined for the current alone case. Steady current around a rotating cylinder was studied experimentally and numerically. Both data sets have been included in Figure 5.16. Figure 5.16 suggests that the lift coefficient in the

current alone case is similar to the lift coefficient determined for the cross-flow current component for large speed ratios.
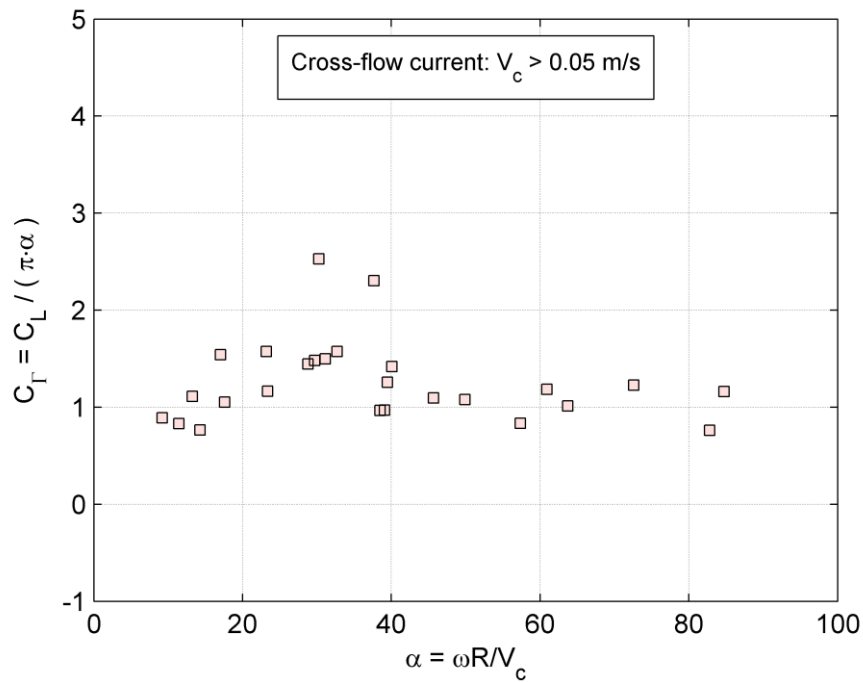
Figure 5.15   Lift coefficient, expressed as C_Γ, determined for the cross-flow current. Mean and standard deviation of C_Γ is 1.16 and 0.26, when disregarding data point where $C_\Gamma > 2$.
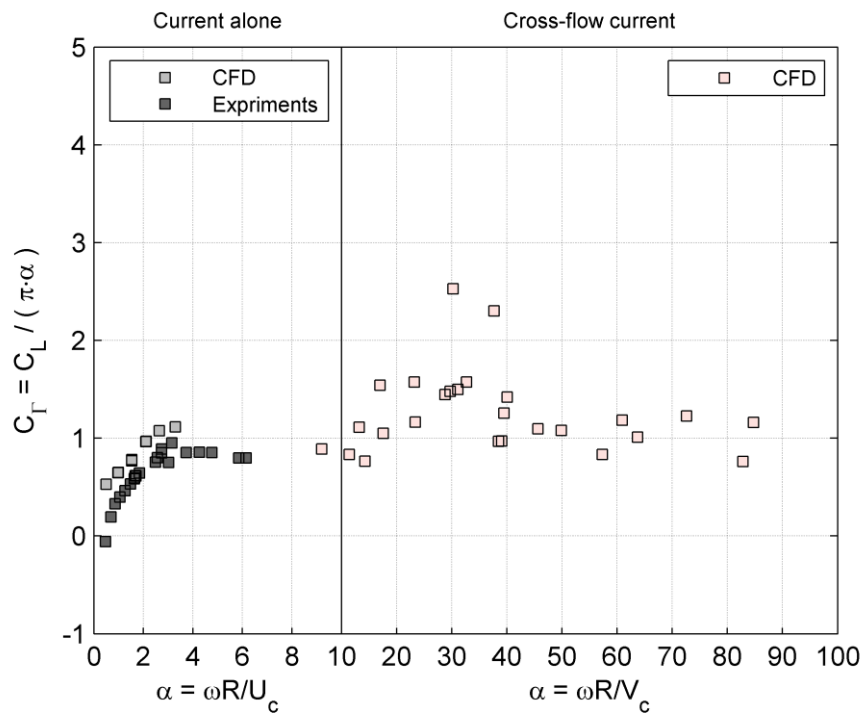
Figure 5.16   Lift coefficient, expressed as C_Γ, in the right pane determined for the cross-flow current and in the left pane determined for steady current around a rotating cylinder.

5.7.2 In-line Force Coefficients

Co-linear Wave and Current Component

The in-line force is determined as for the wave alone case, see Sections 5.1.1 and 5.3. Figure 5.17 shows the measured in-line force expressed as a drag and inertia coefficient (hydrodynamic mass coefficient). In Figure 5.18 the force coefficients are expressed as a ratio to the force coefficients in the wave alone case. There is, as for the case wave with rotation, an indication that the cylinder rotation, i.e. the Magnus effect, could be affecting the in-line drag force. The trend has been indicated in the figure. The in-line hydrodynamic mass force appears not to be affected by cylinder rotation and only limited by the current for the present tested conditions, which are primarily wave-dominated cases.
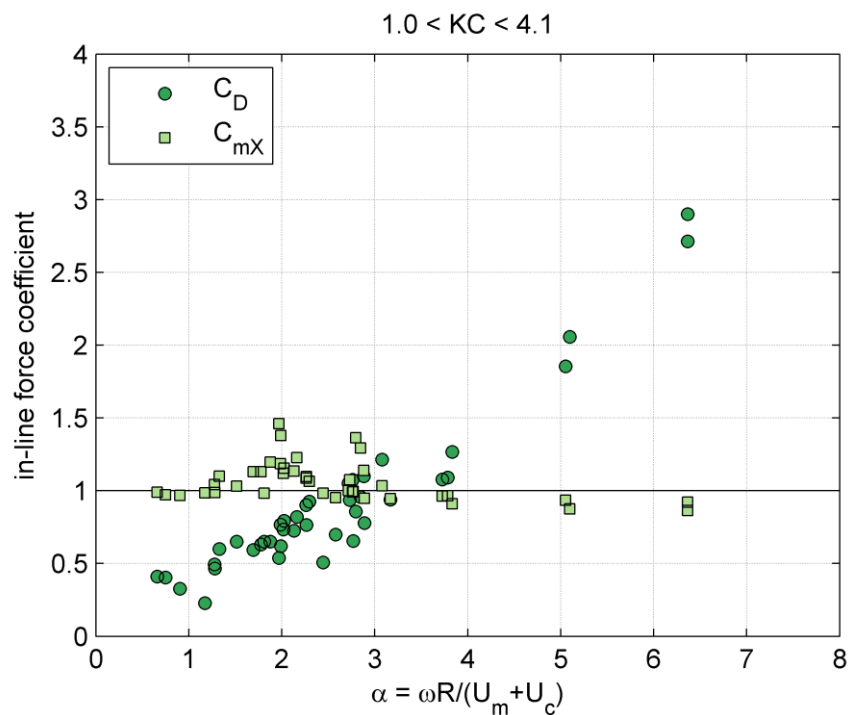
Figure 5.17   Variation of C_D and C_{mX} with KC number for the case co-linear wave and current with rotation.
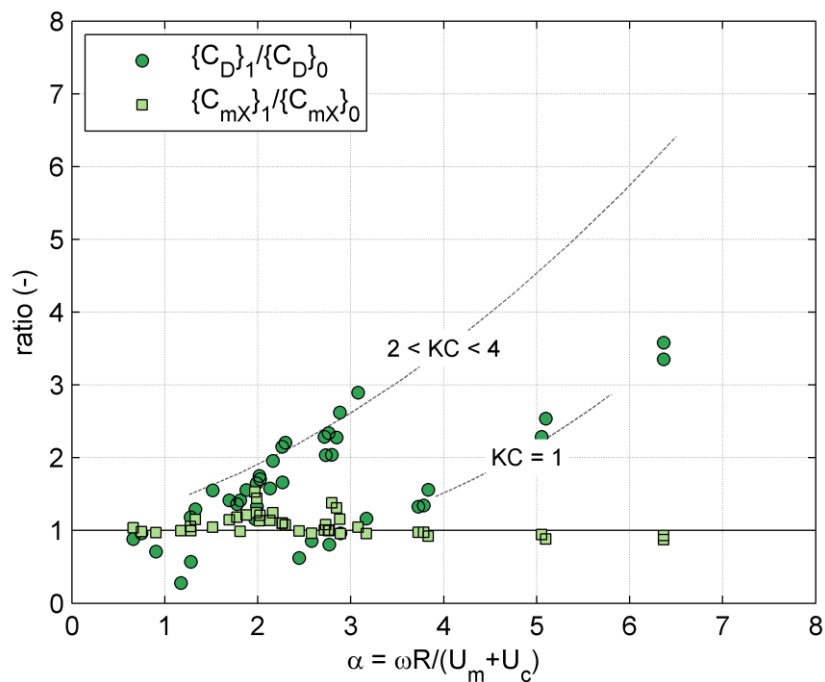
Figure 5.18   *Variation of C_D and C_{mX} with KC number for the case co-linear wave and current with rotation. Indices 1 and 0 represent with and without cylinder rotation and current, respectively. (E.g. $\{C_D\}_0$ is the drag coefficient in waves alone, Figure 5.2). KC number range: $1 < KC < 4.1$.*

Cross-flow Current Component

Figure 5.19 shows the determined drag coefficient for the cross-flow current component. There is a large scatter in the data point, which also makes it difficult to identify a trend. The drag coefficient is, however, believed to increase with increasing speed ratio. Note that the speed ratios are many times larger than those investigated for the case steady current around a rotating cylinder, Section 5.5. This belief is supported by Figure 5.21. Figure 5.21 compares the ratio between the lift and the drag coefficients determined for the cross-flow current component with the same ratio determined for the case steady current around a rotating cylinder. The scatter in the data point for the cross-flow current component is still large. However, seeing beyond the scatter, the ratio between the lift and drag coefficients appears to be independent of the speed ratio for $\alpha > 5$. Given the lift coefficient has been found to increase linearly with the speed ratio, then a constant ratio between the lift and drag coefficient would suggest that the drag coefficient is also increasing linearly with the speed ratio. Figure 5.20 shows the lift/drag ratio for the cross-flow current component in the form of a lift-drag polar plot.
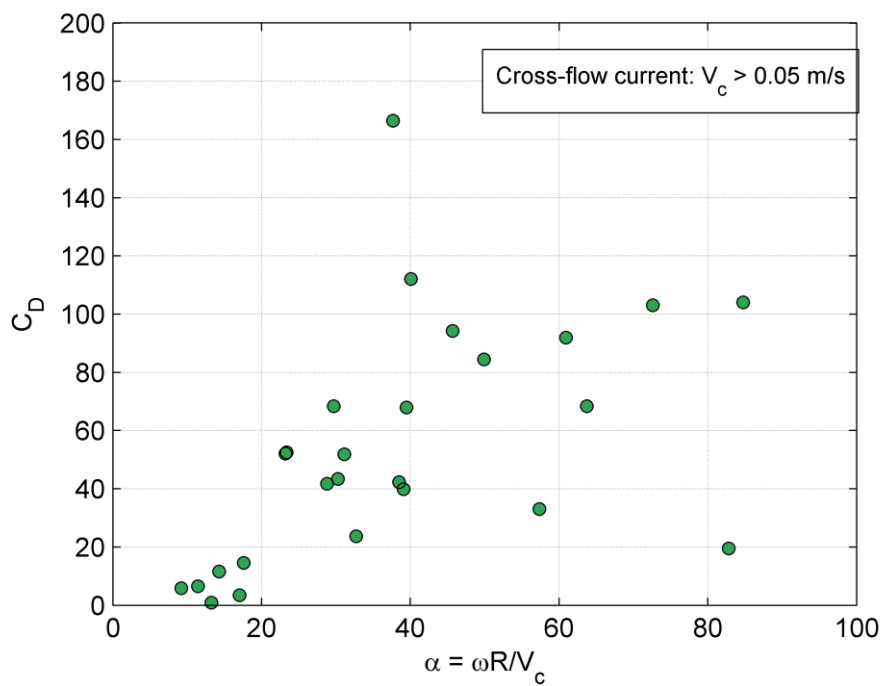
Figure 5.19   The determined drag coefficient, C_D, versus the speed ratio for the cross-flow current components.
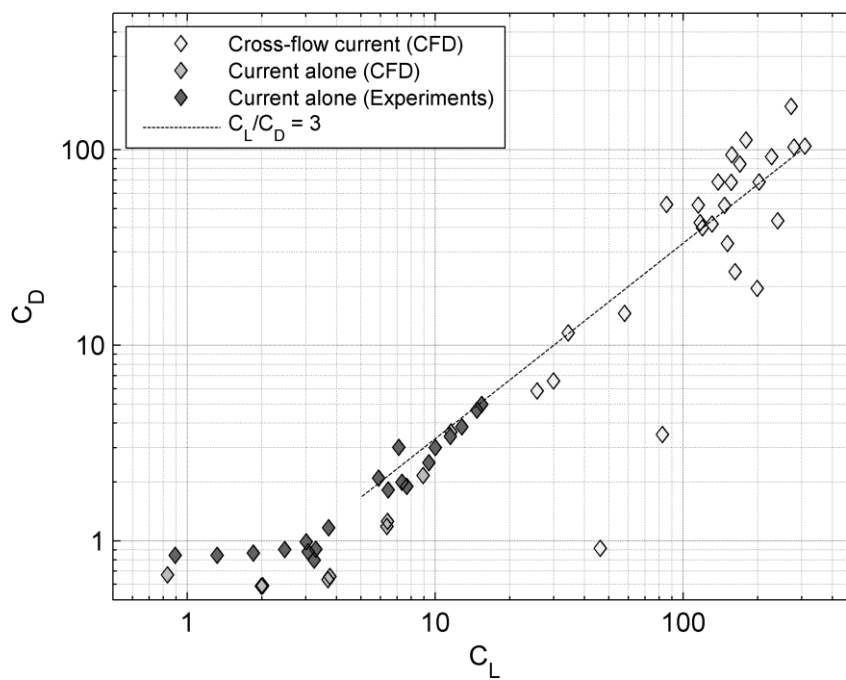
Figure 5.20   Lift-drag polar for the cross-flow current component.
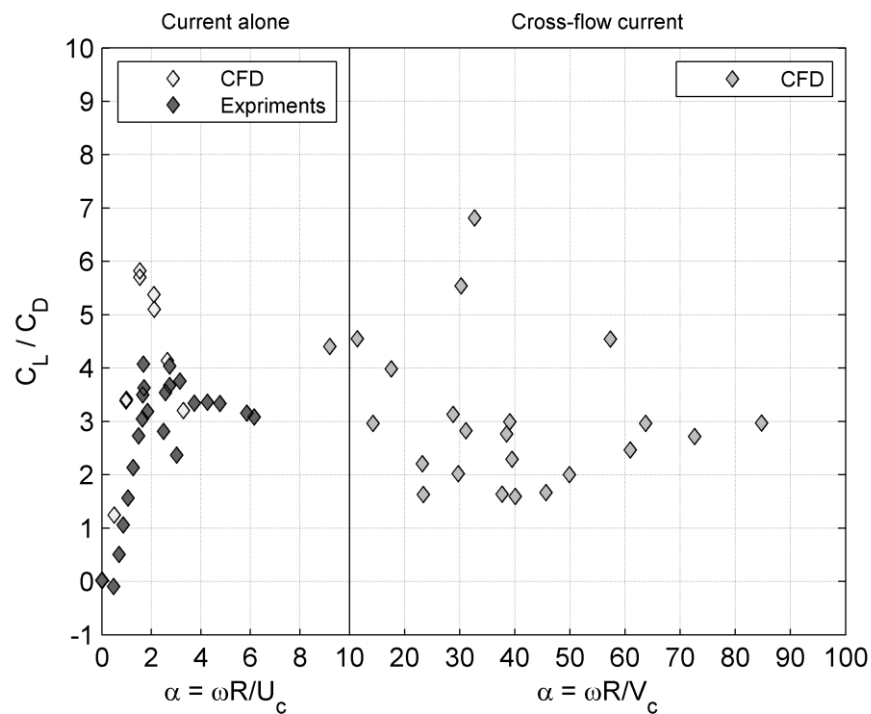
Figure 5.21   Lift/drag ratio versus the speed ratio.

5.7.3   Friction Torque

The average friction torque, Mz (moment) may be represented by the non-dimensional friction coefficient as detailed in Section 5.4. Figure 5.22 shows the measured friction coefficient as a function of Re_ω. Also plotted in the figure are data from Theodorsen & Kegier (1945) /6/. Generally, the friction coefficients for the combined wave and current with rotation case are of the same order of magnitude as those for rotation alone.
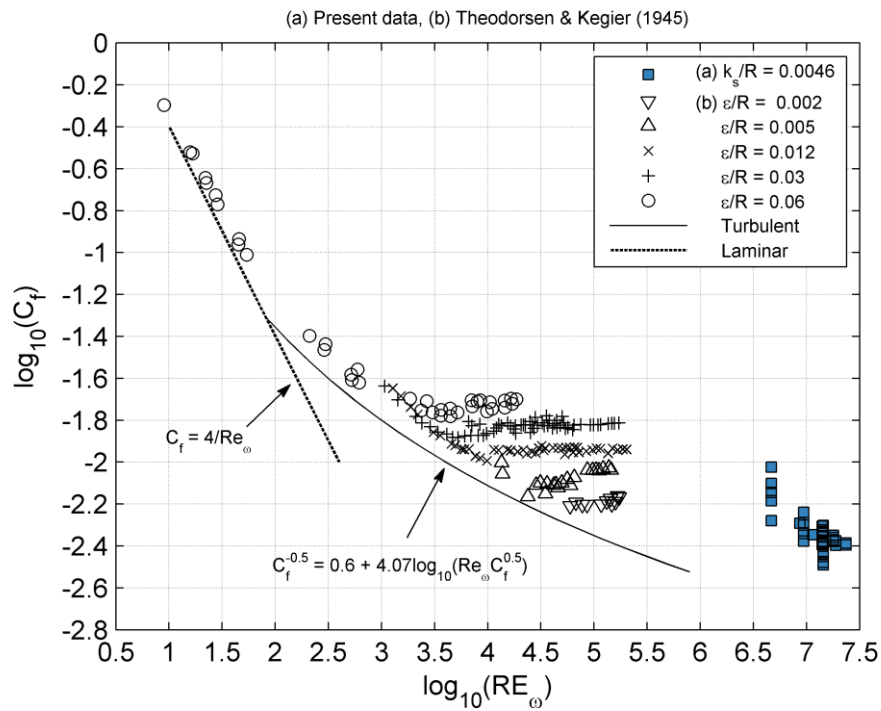
Figure 5.22   *Friction coefficient, C_f, as a function of Re_ω. (a) Solid squares: present data; (b) Other data from Theodorsen & Kegier (1945) /6/. Dotted line: smooth surface, laminar flow. Solid line: smooth surface, turbulent flow.*

6   REFERENCES

/1/   L. Vita, U. S. Paulson, T.F. Pedersen, H.A. Madsen and F. Rasmussen (2009), *A novel floating offshore wind turbine concept*, Proceedings of the 2009 European Wind Energy Conference, Marseille, France.

/2/   Achenbach, E. and Heinecke E. (1981): On vortex shedding from smooth and rough cylinders in the range of Reynolds numbers 6×10^3 to 5×10^6. J. Fluid Mech., 109:239-251.

/3/   Schewe, G. (1983): On the force fluctuations acting on a circular cylinder in cross-flow from subcritical.

/4/   Sarpkaya, T. (1986): Force on a circular cylinder in viscous oscillatory flow at low Keulegan-Carpenter numbers. J. Fluid Mech., 165:61-71.

/5/   Sarpkaya, T. (1976):   In-Line and transverse forces on smooth and sand – roughened cylinders in oscillatory flow at high Reynolds numbers. Naval Post-graduate School, Monterey, CA, Tech. rep. NPS-69SL76062.

/6/   T. Theodorsen and A. Kegier (1945), *Experiments on drag of revolving disks, cylinders, and streamline rods at high speeds*, National Advisory Committee for Aeronautics, Report no. 793.

/7/   DHI report Deliverable 6.1 "Technical Report on the Physical model Exeperiments". Prepared for the DeepWind consortium. February 2012.

/8/   Fuhrman, D.R., Fredsøe, J. and Sumer, D.MN. (2009). Bed slope effect on turbulent wave boundary layers: 1. Model validation and quantification of rough turbulent results. Journal of Geophysical Research, Vol. 113, C03024, 1-16.

/9/   R. I. Basu (1985). *Aerodynamic Forces on Structures of Circular Cross-section. Part 1. Model-scale Data obtained under two-dimensional conditions in low-turbulence streams*. Journal of Wind Engineering and Industrial Aerodynamics, 21, pp 273-294.

/10/   Hoerner, S- F- and H. V. *Borst, Fluid-Dynamic Lift*. Bricktown, NJ: Hoerner Fluid Dynamics, 1975.

/11/   B. M. Sumer and J. Fredsøe (1997), *Hydrodynamics around cylindrical structures*, World Scientific, Advanced Series on Coastal Engineering – Volume 12.

/12/   265679 - DEEPWIND project, *Test plan – Milestone 11 Work Packeage 6*, February 2011. Report prepared by DHI for the DEEPWIND Consortium.

/13/   OpenFOAM User Guide version 1.7.1 (www.openfoam.com)

A P P E N D I X   A

Test Conditions and Force Coefficients

A.1 Current alone

Table A.1   Test conditions and results. Steady current around a fixed cylinder.

Test No.	U_c	Re_c	C_D	C_L
		$= D \cdot U_c / \nu$		
(-)	(m/s)	(-)	(-)	(-)
88.101	0.58	$3.5 \cdot 10^6$	0.79	N/A
88.102	0.36	$2.7 \cdot 10^6$	0.82	N/A
88.103	0.45	$2.2 \cdot 10^6$	0.75	N/A
83.13	0.60	$3.6 \cdot 10^6$	0.76	N/A

A.2 Wave alone

Table A.2   Test conditions and results. Wave alone tests (fixed cylinder).

Test	T	U_m	KC	RE	β	C_D	$C_{m,x}$
			$= U_m T / D$	$= D \cdot U_m / \nu$	$= RE/KC$		
(-)	(s)	(m/s)	(-)	(-)	(-)	(-)	(-)
88.76	11.0	2.25	4.1	$1.4 \cdot 10^7$	$3.3 \cdot 10^6$	0.46	0.96
88.77	9.6	1.94	3.1	$1.2 \cdot 10^7$	$3.8 \cdot 10^6$	0.42	0.99
88.78	7.8	1.59	2.1	$9.5 \cdot 10^6$	$4.6 \cdot 10^6$	0.46	1.00
88.79	5.5	1.13	1.0	$6.8 \cdot 10^6$	$6.6 \cdot 10^6$	0.80	0.99
88.81	14.6	2.97	7.2	$1.8 \cdot 10^7$	$2.5 \cdot 10^6$	0.70	0.82
88.82	15.6	3.18	8.3	$1.9 \cdot 10^7$	$2.3 \cdot 10^6$	0.80	0.72
88.83	16.5	3.38	9.3	$2.0 \cdot 10^7$	$2.2 \cdot 10^6$	0.85	0.61
88.84	12.3	2.52	5.2	$1.5 \cdot 10^7$	$2.9 \cdot 10^6$	0.54	0.92
88.85	3.9	0.81	0.5	$4.9 \cdot 10^6$	$9.2 \cdot 10^6$	1.56	0.98
88.86	2.8	0.58	0.3	$3.5 \cdot 10^6$	$1.3 \cdot 10^7$	3.47	0.96
88.87	13.5	2.75	6.2	$1.7 \cdot 10^7$	$2.7 \cdot 10^6$	0.64	0.85
88.88	12.9	2.63	5.7	$1.6 \cdot 10^7$	$2.8 \cdot 10^6$	0.59	0.89
88.89	15.1	3.08	7.7	$1.9 \cdot 10^7$	$2.4 \cdot 10^6$	0.75	0.76
88.90	17.4	3.56	10.3	$2.1 \cdot 10^7$	$2.1 \cdot 10^6$	0.88	0.44

A.3 Rotation alone

Table A.3   Test conditions and results. Rotation alone tests

Test No.	ω	Re_ω	$\log_{10}(Re_\omega)$	C_f	$\log_{10}(C_f)$
		$= \omega \cdot R^2 / \nu$			
(-)	(rad/s)	(-)	(-)	(-)	(-)
88.97	0.011	99000	5.0	0.0048	-2.32
88.98	0.011	99000	5.0	0.0102	-1.99
88.99	0.00176	15840	4.2	0.0089	-2.05
88.100	0.00442	39780	4.6	0.0104	-1.98

A.4 Current with Rotation

Table A.4   Test conditions and results. Current with rotation tests

Test No.	U_c	Re_c	ω	α	C_D	C_L
		$= D*U_c/\nu$		$=\omega \cdot R/U_c$		
(-)	(m/s)	(-)	(rad/s)	(-)	(-)	(-)
83.08	0.59	$3.5 \cdot 10^6$	-0.52	2.6	2.16	8.92
83.09	0.61	$3.6 \cdot 10^6$	-0.31	1.5	0.66	3.76
83.10	0.57	$3.4 \cdot 10^6$	-0.63	3.3	3.60	11.55
83.11	0.60	$3.6 \cdot 10^6$	-0.42	2.1	1.26	6.41
83.12	0.60	$3.6 \cdot 10^6$	-0.10	0.5	0.67	0.83
83.13	0.60	$3.6 \cdot 10^6$	0.00	0.0	0.76	0.00
83.14	0.61	$3.7 \cdot 10^6$	-0.20	1.0	0.59	2.01
83.22	0.61	$3.7 \cdot 10^6$	-0.31	1.53	0.63	3.68
83.23	0.61	$3.7 \cdot 10^6$	-0.20	0.98	0.59	1.99
83.24	0.60	$3.6 \cdot 10^6$	-0.42	2.10	1.18	6.37

A.5 Wave with Rotation

Table A.5   Test conditions and results. Wave with rotation tests

Test	T	U_m	KC =	Re =	ω	α	C_D	$C_{m,X}$	C_Γ	$C_{m,Y}$
			$U_m \cdot T/D$	$D \cdot U_m/\nu$		$\omega R/U_m$				
(-)	(s)	(m/s)	(-)	(-)	rad/s	(-)	(-)	(-)	(-)	(-)
83.15	11.0	2.25	4.1	$1.35 \cdot 10^7$	-1.05	1.40	0.67	1.00	0.99	0.12
83.16	11.0	2.25	4.1	$1.35 \cdot 10^7$	-0.52	0.69	0.46	0.96	1.34	0.05
83.17	11.0	2.25	4.1	$1.35 \cdot 10^7$	0.00	0.00	0.46	0.95	0.00	0.00
83.18	9.6	1.95	3.1	$1.17 \cdot 10^7$	-3.15	4.85	1.80	1.16	0.51	0.32
83.19	7.8	1.59	2.1	$9.56 \cdot 10^6$	-3.15	5.93	2.60	0.97	0.51	0.35
83.20	5.5	1.13	1.0	$6.77 \cdot 10^6$	-2.05	5.45	2.07	0.86	0.52	0.13
88.01	11.0	2.25	4.1	$1.35 \cdot 10^7$	1.60	2.13	0.85	1.07	0.76	0.17
88.02	9.6	1.95	3.1	$1.17 \cdot 10^7$	1.60	2.46	1.02	0.97	0.76	0.17
88.03	7.8	1.59	2.1	$9.56 \cdot 10^6$	1.60	3.01	1.28	0.87	0.71	0.15
88.04	5.5	1.13	1.0	$6.76 \cdot 10^6$	1.60	4.26	1.35	0.90	0.52	0.08
88.57	3.9	0.80	0.5	$4.80 \cdot 10^6$	1.60	6.00	1.43	0.95	0.44	0.03
88.93	9.6	1.95	3.1	$1.17 \cdot 10^7$	2.00	3.08	1.23	1.01	0.67	0.21
83.28	11.0	2.47	4.5	$1.48 \cdot 10^7$	-1.57	1.91	0.78	1.10	0.80	0.16
83.29	11.0	2.96	5.4	$1.78 \cdot 10^7$	-1.57	1.59	0.65	1.20	0.85	0.15
83.30	11.0	1.98	3.6	$1.19 \cdot 10^7$	-1.57	2.38	0.97	1.03	0.75	0.18
83.31	12.0	2.96	5.9	$1.78 \cdot 10^7$	-2.10	2.13	0.62	1.27	0.61	0.16
83.32	8.0	2.25	3.0	$1.35 \cdot 10^7$	-1.05	1.40	0.91	0.94	1.26	0.14

A.6 Combined Wave and Current with Rotation

Table A.6   Test conditions and results. Combined wave and current with rotation tests. Co-linear wave and current component

Test	T	U_m	KC = $U_m \cdot T/D$	U_c	ω	α = $\omega R/(U_m+U_c)$	C_D	$C_{m,X}$	C_Γ	$C_{m,Y}$
(-)	(s)	(m/s)	(-)	(m/s)	rad/s	(-)	(-)	(-)	(-)	(-)
88.05	11.0	2.25	4.1	0.16	1.60	1.99	0.62	1.38	-0.89	-0.16
88.06	9.6	1.95	3.1	0.28	1.60	2.16	0.82	1.23	-0.94	-0.20
88.07	7.8	1.59	2.1	0.17	1.60	2.73	0.94	1.08	-0.88	-0.12
88.08	5.5	1.13	1.0	0.38	1.60	3.17	0.94	0.95	-0.78	-0.05
88.09	11.0	2.25	4.1	0.18	1.60	1.97	0.54	1.46	-0.93	-0.17
88.10	9.6	1.94	3.1	0.44	1.60	2.02	0.73	1.12	-0.92	-0.13
88.11	7.8	1.59	2.1	0.53	1.60	2.27	0.76	1.10	-0.98	-0.13
88.12	5.5	1.13	1.0	0.53	1.60	2.89	0.78	0.95	-0.85	-0.04
88.13	11.0	2.25	4.1	0.12	1.60	2.02	0.79	1.15	-0.79	-0.16
88.14	9.6	1.95	3.1	0.14	1.60	2.30	0.93	1.06	-0.81	-0.15
88.15	7.8	1.59	2.1	0.14	1.60	2.76	1.08	0.99	-0.82	-0.13
88.16	5.5	1.13	1.0	0.14	1.60	3.78	1.09	0.96	-0.70	-0.06
88.17	11.0	2.23	4.1	0.47	1.60	1.77	0.63	1.13	-0.92	-0.19
88.18	9.6	1.95	3.1	0.61	1.60	1.88	0.65	1.20	-1.06	-0.30
88.19	7.8	1.59	2.1	0.66	1.60	2.13	0.72	1.13	-1.09	-0.15
88.20	5.5	1.13	1.0	0.60	1.60	2.77	0.66	1.00	-0.98	-0.03
88.91	9.6	1.95	3.1	0.32	1.28	1.69	0.59	1.13	-1.04	-0.14
88.92	9.6	1.95	3.1	0.31	0.96	1.27	0.49	1.04	-1.17	-0.12
88.93	9.6	1.95	3.1	0.00	2.00	3.08	1.21	1.03	-0.67	-0.20
88.94	9.6	1.95	3.1	0.16	2.00	2.85	0.96	1.29	-0.77	-0.18
88.95	9.6	1.95	3.1	0.20	2.00	2.79	0.86	1.36	-0.80	-0.18
88.96	9.6	1.95	3.1	0.13	2.00	2.88	1.10	1.14	-0.71	-0.19
83.33	11.0	2.25	4.1	0.12	-1.57	1.99	0.77	1.19	0.82	0.16
83.34	9.6	1.95	3.1	0.14	-1.57	2.26	0.90	1.09	0.83	0.15
83.35	7.8	1.59	2.1	0.14	-1.57	2.72	1.05	1.00	0.84	0.13
83.36	5.5	1.13	1.0	0.14	-1.57	3.73	1.08	0.96	0.71	0.06
83.37	11.0	2.25	4.1	0.12	-1.05	1.33	0.60	1.10	1.04	0.11
83.38	9.6	1.95	3.1	0.13	-1.05	1.51	0.65	1.03	1.05	0.10
83.39	7.8	1.59	2.1	0.15	-1.05	1.81	0.65	0.98	1.02	0.07
83.40	5.5	1.13	1.0	0.16	-1.05	2.44	0.51	0.98	0.86	0.03
83.41	11.0	2.25	4.1	0.11	-0.52	0.66	0.41	0.99	1.34	0.06
83.42	9.6	1.95	3.1	0.14	-0.52	0.75	0.40	0.97	1.34	0.05
83.43	7.8	1.59	2.1	0.14	-0.52	0.90	0.33	0.97	1.09	0.03
83.44	5.5	1.12	1.0	0.21	-0.52	1.17	0.23	0.99	0.94	0.01
83.45	5.5	1.12	1.0	0.10	-0.52	1.28	0.46	0.99	0.48	0.01
83.46	5.5	1.12	1.0	0.10	-1.05	2.58	0.70	0.95	0.58	0.03
83.47	5.5	1.13	1.0	0.10	-1.57	3.83	1.27	0.91	0.57	0.07
83.48	5.5	1.13	1.0	0.11	-2.1	5.10	2.06	0.87	0.54	0.13
83.49	5.5	1.13	1.0	0.12	-2.1	5.05	1.86	0.94	0.63	0.12
83.50	5.5	1.13	1.0	0.11	-2.62	6.36	2.90	0.87	0.52	0.20
83.51	5.5	1.13	1.0	0.11	-2.62	6.36	2.71	0.92	0.57	0.19

Table A.7   Test conditions and results. Combined wave and current with rotation tests. Cross-flow current component.

Test	T	U_m	KC = $U_m \cdot T/D$	V_c	ω	α = $\omega R/(V_c)$	C_D	C_L
(-)	(s)	(m/s)	(-)	(m/s)	rad/s	(-)	(-)	(-)
88.05	11.0	2.25	4.1	-0.16	1.60	-29.7	-68.45	-138.17
88.06	9.6	1.95	3.1	-0.07	1.60	-71.4	N/A	N/A
88.07	7.8	1.59	2.1	-0.17	1.60	-28.8	-41.76	-130.66
88.08	5.5	1.13	1.0	-0.34	1.60	-14.3	11.58	-34.28
88.09	11.0	2.25	4.1	-0.21	1.60	-23.2	-52.10	-114.80
88.10	9.6	1.94	3.1	-0.27	1.60	-17.6	14.57	-58.01
88.11	7.8	1.59	2.1	-0.15	1.60	-32.7	-23.73	-161.73
88.12	5.5	1.13	1.0	-0.42	1.60	-11.4	6.57	-29.89
88.13	11.0	2.25	4.1	-0.04	1.60	-119.1	N/A	N/A
88.14	9.6	1.95	3.1	-0.06	1.60	-84.8	-104.09	-309.00
88.15	7.8	1.59	2.1	-0.10	1.60	-49.9	-84.45	-169.02
88.16	5.5	1.13	1.0	-0.12	1.60	-39.1	-39.86	-119.22
88.17	11.0	2.23	4.1	-0.28	1.60	-17.0	3.50	-82.32
88.18	9.6	1.95	3.1	-0.05	1.60	-98.3	N/A	N/A
88.19	7.8	1.59	2.1	-0.13	1.60	-37.7	-166.45	-272.49
88.20	5.5	1.13	1.0	-0.52	1.60	-9.2	5.84	-25.72
88.91	9.6	1.95	3.1	-0.05	1.28	-80.1	N/A	N/A
88.92	9.6	1.95	3.1	-0.10	0.96	-30.3	-43.37	-240.38
88.93	9.6	1.95	3.1	0.00	2.00	3553.1	N/A	N/A
88.94	9.6	1.95	3.1	-0.15	2.00	-39.5	-68.01	-155.84
88.95	9.6	1.95	3.1	-0.19	2.00	-31.1	-51.88	-146.39
88.96	9.6	1.95	3.1	-0.09	2.00	-63.7	-68.36	-202.34
83.33	11.0	2.25	4.1	0.06	-1.57	72.6	103.03	-279.55
83.34	9.6	1.95	3.1	0.08	-1.57	60.9	92.01	-226.91
83.35	7.8	1.59	2.1	0.10	-1.57	45.7	94.30	-157.15
83.36	5.5	1.13	1.0	0.12	-1.57	38.5	42.35	-116.94
83.37	11.0	2.25	4.1	0.01	-1.05	396.7	N/A	N/A
83.38	9.6	1.95	3.1	0.04	-1.05	71.8	N/A	N/A
83.39	7.8	1.59	2.1	0.08	-1.05	40.1	112.15	-178.73
83.40	5.5	1.13	1.0	0.13	-1.05	23.4	52.55	-85.49
83.41	11.0	2.25	4.1	-0.01	-0.52	-146.1	N/A	N/A
83.42	9.6	1.95	3.1	-0.02	-0.52	-86.9	N/A	N/A
83.43	7.8	1.59	2.1	-0.00	-0.52	-879.6	N/A	N/A
83.44	5.5	1.12	1.0	0.12	-0.52	13.2	0.92	-46.16
83.45	5.5	1.12	1.0	0.00	-0.52	600.0	N/A	N/A
83.46	5.5	1.12	1.0	-0.01	-1.05	-541.0	N/A	N/A
83.47	5.5	1.13	1.0	0.00	-1.57	1023.6	N/A	N/A
83.48	5.5	1.13	1.0	0.02	-2.1	292.0	N/A	N/A
83.49	5.5	1.13	1.0	0.11	-2.1	57.3	33.10	-150.36
83.50	5.5	1.13	1.0	0.04	-2.62	210.0	N/A	N/A
83.51	5.5	1.13	1.0	0.09	-2.62	82.8	19.56	-198.27